

# On the Formation and Progenitor of PSR J0737-3039: New Constraints on the Supernova Explosion Forming Pulsar B

B. Willems,<sup>\*</sup> J. Kaplan,<sup>†</sup> T. Fragos,<sup>‡</sup> and V. Kalogera<sup>§</sup>

*Northwestern University, Department of Physics and Astronomy, 2145 Sheridan Road, Evanston, IL 60208, USA*

K. Belczynski<sup>¶</sup>

*New Mexico State University, Department of Astronomy,  
1320 Frenger Mall, Las Cruces, NM 88003, USA  
Tombaugh Fellow*

We investigate the formation of the double pulsar PSR J0737-3039 and examine its most likely progenitors, taking into account the most recent and all currently available observational constraints. We show that the most likely kick velocity and progenitor parameters depend strongly on the consideration of the full five-dimensional probability distribution function for the magnitude and direction of the kick velocity imparted to pulsar B at birth, the mass of pulsar B's pre-supernova helium star progenitor, and the pre-supernova orbital separation rather than marginalized one- or two-dimensional distributions for the kick velocity and progenitor mass. The priors that enter the analysis are the age of the system, the minimum helium star mass required to form a neutron star, the transverse systemic velocity, and the treatment of the unknown radial velocity. Since the latter cannot be measured observationally, we adopt a statistical approach and use theoretical radial-velocity distributions obtained from population synthesis calculations for coalescing double neutron stars. We find that when the minimum pre-supernova helium star mass required for neutron star formation is assumed to be  $2.1 M_{\odot}$ , the most likely kick velocity ranges from  $70 \text{ km s}^{-1}$  to  $180 \text{ km s}^{-1}$ . When, on the other hand, masses lower than  $2.1 M_{\odot}$  are allowed as neutron star progenitors, the most likely kick velocity can reach very low values (as low as a few  $\text{km s}^{-1}$ ), although the majority of the models still yield most likely kick velocities of  $50 \text{ km s}^{-1}$  to  $170 \text{ km s}^{-1}$ . Hence, we agree with Piran & Shaviv [19] that the observed system properties, including the low transverse systemic velocity, *can* indeed be compatible with low progenitor masses and low kick velocities. Equally important though, we show that this is not the only likely formation path of pulsar B, due to the role of different prior assumptions that are necessary in the analysis. Moreover, in contrast to earlier claims in the literature, we show that the proximity of the double pulsar to the Galactic plane and the small proper motion do not pose stringent constraints on the kick velocity and progenitor mass of pulsar B at all. Instead, the constraints imposed by the current orbital semi-major axis and eccentricity and the orbital dynamics of asymmetric supernova explosions turn out to be much more restrictive. We conclude that without further knowledge of the priors, the currently available observational constraints cannot be used to unambiguously favor a specific core-collapse and neutron star formation mechanism. Both electron capture and neutrino-driven supernovae therefore remain viable formation mechanisms for pulsar B.

PACS numbers: 97.60.Bw,97.60.Gb,97.80.-d

## I. INTRODUCTION

Since its discovery in 2003 [1, 2], the double pulsar PSR J0737-3039 has proven to be an extraordinary system for the study of both fundamental physics and general relativity [3, 4]. The system is highly relativistic with an orbital period of 2.4 hrs and an eccentricity of 0.0878, making it the tightest known double neutron star (DNS) binary known to date. The system also harbors the fastest known DNS pulsar (22.7 ms), has the largest apsidal-motion rate of all presently known DNSs

( $16.9^{\circ} \text{ yr}^{-1}$ ), and shows eclipses of the fast pulsar by the magnetosphere of the slow one (orbital inclination  $i = 87^{\circ} \pm 3^{\circ}$ ) [1, 2]. Its short merger time of  $\sim 85 \text{ Myr}$  has furthermore led to a significant upward revision for the merger rate of coalescing DNSs [5, 6].

A central topic in understanding the physics of the double pulsar is the study of its origin and evolution. According to our current knowledge (for more details see [7–10]), DNSs form from primordial binaries in which, possibly after some initial mass-transfer phase, both component stars have masses in excess of  $\sim 8 - 12 M_{\odot}$ . After the primary explodes in a supernova (SN) explosion to form the first neutron star (NS), the binary enters a high-mass X-ray binary phase in which the NS accretes matter from the wind of its companion. The phase ends when the companion star evolves off the main sequence and engulfs the NS in its expanding envelope. The NS then spirals in towards the core of the companion until

<sup>\*</sup>Electronic address: b-willems@northwestern.edu

<sup>†</sup>Electronic address: j-kaplan-1@northwestern.edu

<sup>‡</sup>Electronic address: tassosfragos@northwestern.edu

<sup>§</sup>Electronic address: vicky@northwestern.edu

<sup>¶</sup>Electronic address: kbelczyn@nmsu.edu

enough orbital energy is transferred to the envelope to expel it from the system. When the envelope is ejected, the binary consists of the NS and the stripped-down helium core of its former giant companion, orbiting each other in a tight orbit. If the NS is able to accrete during its rapid inspiral, a first "recycling" may take place during which it is spun up to millisecond periods. The helium star then evolves further until it, in turn, explodes and forms a NS. Depending on the mass of the helium star and the size of the orbit at the time of the explosion, the SN may be preceded by a second recycling phase when the helium star fills its Roche lobe and transfers mass to the NS [9, 11, 12].

Shortly after the discovery of PSR J0737-3039, Dewi & van den Heuvel [13] and Willems & Kalogera [14] (hereafter Paper I) independently derived that, right before the second SN explosion, the binary was so tight that the helium star must have been overflowing its critical Roche lobe. This conclusion, for the first time, strongly confirmed the above formation channel for DNS binaries. The observed 22.7 ms pulsar (hereafter PSR J0737-3039A or pulsar A) then corresponds to the first-born NS, and its 2.8 s pulsar companion (hereafter PSR J0737-3039B or pulsar B) to the second-born NS.

In a follow-up study to Paper I, Willems et al. [15] (hereafter Paper II) extended the stellar and binary evolution constraints on the formation of pulsar B to include constraints based on the system's position and motion in the Galaxy. While the addition of proper motion measurements to the list of observational constraints, at first sight, added a significant piece of information on the formation and evolution of the double pulsar system, the unknown direction of the proper motion and the unknown radial velocity significantly hindered the derivation of more stricter progenitor constraints than obtained in Paper I.

Since Paper II, the available observational constraints have undergone significant revisions. Most notably, proper motion estimates, which form a vital part in constraining the kick imparted to pulsar B at birth, have decreased from  $\sim 141 \text{ km s}^{-1}$  down to  $\sim 30 \text{ km s}^{-1}$  or less [4, 16, 17]. In addition, rough limits on the spin-orbit misalignment of pulsar A have recently been derived by Manchester et al. [18], which again add to the constraints on pulsar B's natal kick velocity. From a theoretical point of view, it has furthermore been argued that pulsar B may have had an unusually low-mass progenitor ( $\sim 1.45 M_{\odot}$ ) which formed a NS through a new type of gravitational collapse accompanied by an unusually low kick velocity ( $\lesssim 30 \text{ km s}^{-1}$ ) [19, 20].

Our aim in this paper is to investigate the system's recent evolutionary history and examine the necessity of this new type of gravitational collapse to explain the formation of pulsar B. We incorporate the most up-to-date observational information on PSR J0737-3039, including the  $30 \text{ km s}^{-1}$  upper limit on the proper motion derived by Kramer et al. [4]. A significant new element compared to Papers I and II, which focused on the extent of

the available parameter space, is the examination of the full multi-dimensional probability distribution functions (PDF) for the magnitude and direction of pulsar B's natal kick velocity, the mass of pulsar B's pre-SN helium star progenitor, and the orbital separation right before the formation of pulsar B. Other significant improvements are the incorporation of theoretical distribution functions for the unknown radial velocity by means of binary population synthesis calculations for coalescing DNSs, the investigation of projection and marginalization effects of the multi-dimensional PDF, and the examination of the role of the prior assumptions.

The plan of the paper is as follows. In § II, we briefly summarize the observationally inferred properties of the double pulsar relevant to this investigation. In § III, we present the basic assumptions and outline the method used to derive the formation history of pulsar B. Details of the various steps adopted in the investigation and their overall role in the analysis are presented in § IV and § V. In § VI, we present the most likely progenitor and formation parameters for PSR J0737-3039B and systematically explore the sensitivity of the parameters to the adopted assumptions. The final two sections, § VII and § VIII, are devoted to a comparison with previous investigations and summarizing remarks.

## II. OBSERVATIONAL CONSTRAINTS

The main properties of the double pulsar system and its component stars relevant to this investigation are summarized in Table I. The principal differences with the observational constraints used in Paper II are the considerably lower estimate for the systemic velocity perpendicular to the line-of-sight, and the availability of limits on the spin-orbit misalignment angle of pulsar A.

The kinematic properties of PSR J0737-3039 have undergone significant revision since Ransom et al. [16] used interstellar scintillation measurements and inferred a velocity component perpendicular to the line-of-sight of  $\sim 141 \text{ km s}^{-1}$ . Coles et al. [17] derived a reduced velocity of  $\sim 66 \text{ km s}^{-1}$  by incorporating anisotropies of the interstellar medium in the interstellar scintillation model. This reduced velocity, however, strongly depends on the adopted anisotropy model. Kramer et al. [4], on the other hand, used pulsar timing measurements to derive a firm model-independent upper limit of  $30 \text{ km s}^{-1}$  on the transverse velocity. In view of these revisions, we update the kinematic properties of PSR J0737-3039 derived in Paper II, adopting the most recent constraint of  $30 \text{ km s}^{-1}$  as an upper limit to the velocity component transverse to the line-of-sight.

The kick imparted to pulsar B at birth is expected to tilt the orbital plane and misalign pulsar A's spin axis with respect to the post-SN orbital angular momentum axis [e.g. 22]. The degree of misalignment depends on both the magnitude and the direction of the kick, and therefore yields a valuable piece of information on pul-

TABLE I: Physical properties of PSR J0737-3039.

| Parameter                                 | Notation           | Value             | Reference |
|---|--------------------|-------------------|-----------|
| Distance (pc)                             | $d$                | 600               | [1, 2]    |
| Galactic longitude (J2000) (deg)          | $l$                | 245.2             | [1, 2]    |
| Galactic latitude (J2000) (deg)           | $b$                | -4.5              | [1, 2]    |
| Proper motion ( $\text{km s}^{-1}$ )      | $V_t$              | $< 30$            | [4]       |
| Spin period of pulsar A (ms)              | $P_A$              | 22.7              | [1, 2]    |
| Spin period of pulsar B (s)               | $P_B$              | 2.8               | [1, 2]    |
| Mass of pulsar A ( $M_\odot$ )            | $M_A$              | 1.34              | [1, 2]    |
| Mass of pulsar B ( $M_\odot$ )            | $M_B$              | 1.25              | [1, 2]    |
| Characteristic age of pulsar A (Myr)      | $\tau_A$           | 210               | [1, 2]    |
| Characteristic age of pulsar B (Myr)      | $\tau_B$           | 50                | [1, 2]    |
| Spin-down age of pulsar A (Myr)           | $\tau_{\text{sd}}$ | 100               | [1, 2]    |
| Spin-orbit misalignment of pulsar A (deg) | $\lambda$          | $< 60$ or $> 120$ | [18]      |
| Orbital period (hours)                    | $P_{\text{orb}}$   | 2.4               | [1, 2]    |
| Orbital semi-major axis ( $R_\odot$ )     | $A_c$              | 1.26              | [1, 2]    |
| Orbital eccentricity                      | $e_c$              | 0.0878            | [1, 2]    |

sar B’s natal kick velocity (see §VB for more details). In Paper II, we showed that for the pre- and post-SN orbital parameters compatible with all available observational constraints, misalignment angles between approximately  $70^\circ$  and  $110^\circ$  are highly unlikely. Manchester et al. [18] derived observational constraints on the spin-orbit misalignment based on the stability of pulsar A’s mean pulse profile over a time span of 3 years. The authors concluded the angle to be smaller than  $\sim 60^\circ$  or larger than  $\sim 120^\circ$ , in agreement with the theoretical predictions of Paper II. In the present paper, we therefore include the limits on pulsar A’s spin-orbit misalignment inferred by Manchester et al. [18] in the list of available observational constraints.

Among the constraints inferred from observations, the most uncertain parameter affecting the reconstruction of the system’s formation and evolutionary history is its age. Characteristic ages, defined as half the ratio of the spin period to the spin-down rate, are the most commonly adopted age estimators, but are known to be quite unreliable [e.g. 23]. In the case of PSR J0737-3039, the spin evolution of pulsar B is furthermore very likely affected by torques exerted by pulsar A on pulsar B [24], adding to the uncertainties of its age. Lorimer et al. [25] therefore derived an alternative age estimate by noting that, according to the standard DNS formation channel, the time expired since the end of pulsar A’s spin-up phase should be equal to the time expired since the birth of pulsar B. By combining this property with a selection of different spin-down models, the authors derived a *most likely* age of 30-70 Myr, but were unable to firmly exclude younger and older ages. A third age estimate can be obtained by assuming that pulsar A was recycled to the maximum spin rate and calculating the time required for it to spin down to the currently observed value. This so-called spin-down age provides an upper limit to the age of the system of 100 Myr [1]. In view of these uncertainties, we derive constraints on the formation and evolution of PSR J0737-3039 for three different sets of

age assumptions: (i)  $0 \leq \tau \leq 100$  Myr (the age range adopted in Papers I and II), (ii)  $30 \leq \tau \leq 70$  Myr (the most likely age range derived by Lorimer et al. [25]), and (iii)  $\tau \simeq 50$  Myr (the characteristic age of pulsar B).

### III. BASIC ASSUMPTIONS AND OUTLINE OF THE CALCULATION

Our goal in this investigation is to reconstruct the evolutionary history of PSR J0737-3039 and constrain its properties at the formation time of pulsar B. More specifically, our aim is to derive a PDF for the magnitude and direction of the kick velocity imparted to pulsar B at birth, the mass of pulsar B’s progenitor immediately before it explodes in a SN explosion, and the orbital separation of the component stars right before the SN explosion. Adopting the standard DNS formation channel, the progenitor of the double pulsar right before the formation of pulsar B, consists of the first-born NS, pulsar A, and the helium star progenitor of the second-born NS. Since the formation of the second NS is preceded by one or more mass-transfer phases, tidal forces can safely be assumed to circularize the orbit prior to the formation of pulsar B. For the remainder of the paper, we refer to the times right before and right after the formation of pulsar B by pre-SN and post-SN, respectively. The subsequent analysis consists of four major parts.

Firstly, the motion of the system in the Galaxy is traced back in time up to a maximum age of 100 Myr. The goal of this calculation is to derive the position and center-of-mass velocity of the binary right after the formation of pulsar B, and use this information to constrain the kick imparted to it at birth. In order to determine possible birth sites, our analysis is supplemented with the assumptions that the primordial DNS progenitor was born close to the Galactic plane, and that the first SN explosion did not kick the binary too far out of it. The first assumption is conform with our current knowledge that

massive stars form and live close to the Galactic plane (their typical scale height is  $\simeq 50\text{--}70\text{ pc}$ ). The second assumption on the other hand neglects a small fraction of systems formed with high space velocities [9, 26] [52]. Under these assumptions, the binary is still close to the Galactic plane at the formation time of pulsar B. Possible birth sites can thus be obtained by calculating the motion in the Galaxy backwards in time and looking for crossings of the orbit with the Galactic mid-plane. The times in the past at which the plane crossings occur yield kinematic estimates for the age of the DNS, while comparison of the system’s total center-of-mass velocity with the local Galactic rotational velocity at the birth sites yields the system’s post-SN *peculiar* velocity.

Secondly, the orbital semi-major axis and eccentricity right after the SN explosion forming pulsar B are determined by integrating the equations governing the evolution of the orbit due to gravitational wave emission backwards in time. The integration is performed for each Galactic plane crossing found from the Galactic motion calculations. Since each crossing yields a different kinematic age, and thus a different endpoint of the reverse orbital evolution calculation, the post-SN parameters are a function of the considered Galactic plane crossing.

Thirdly, the conservation laws of orbital energy and angular momentum are used to map the post-SN binary parameters to the pre-SN ones. The mapping depends on the kick velocity imparted to pulsar B at birth and results in constraints on the magnitude and direction of the kick velocity, the mass of pulsar B’s pre-SN helium star progenitor, and the pre-SN orbital separation. The pre-SN orbital eccentricity is assumed to be zero, as expected from strong tidal forces operating on the binary during the mass-transfer phase(s) responsible for spinning up pulsar A. The kick and pre- and post-SN binary parameters are then furthermore subjected to the requirements that they be consistent with the post-SN peculiar velocity obtained from the Galactic motion calculations and with the observationally inferred spin-orbit misalignment angle of pulsar A. The latter constraint requires the additional assumption that tidal forces align the pre-SN rotational angular momentum vector of pulsar A with the pre-SN orbital angular momentum vector.

Fourthly, the solutions of the conservation laws of orbital energy and angular momentum are weighted according to the likelihood that they lead to the system’s currently observed position and velocity in the Galaxy. A PDF of the admissible kick velocity and progenitor parameters is then constructed by binning the solutions in a multi-dimensional “rectangular” grid. The maximum of the resulting PDF yields the most likely magnitude and direction of the kick velocity imparted to pulsar B at birth, mass of pulsar B’s pre-SN helium star progenitor, and pre-SN orbital separation. We also investigate the sensitivity of the PDF to the adopted assumptions by systematically varying the underlying assumptions, such as, e.g., the age and the magnitude of the transverse systemic velocity component.

## IV. KINEMATIC AGE AND HISTORY

### A. Galactic motion

Tracing the motion of PSR J0737-3039 back in time requires the knowledge of both its present-day position and 3-dimensional space velocity. Unfortunately, no method is presently available to measure radial velocities of DNSs, so that the knowledge of their space velocity is limited to the component perpendicular to the line-of-sight (transverse velocity). At present, only an upper limit is available for the double pulsar:  $V_t \lesssim 30\text{ km s}^{-1}$ . The direction of the motion in the plane perpendicular to the line-of-sight is still unknown. Therefore, as in Paper II, we explore the system’s kinematic history in terms of two unknown parameters: (i) the radial component  $V_r$  of the present-day systemic velocity, and (ii) the orientation  $\Omega$  of the transverse velocity in the plane perpendicular to the line-of-sight. Since the results presented in this paper do not depend on the exact definition of  $\Omega$ , we refer the reader to Paper II for a more detailed discussion and definition.

The motion of the system in the Galaxy is calculated with respect to a right-handed frame of reference  $OXYZ$  with origin at the Galactic center and with the  $XY$ -plane coinciding with the Galactic mid-plane. The  $X$ -axis is chosen such that the Sun is located in the  $XZ$ -plane, and the positive direction of the  $Y$ -axis such that it coincides with the direction of the Galactic rotational velocity at the position of the Sun. The velocity components  $V_X$ ,  $V_Y$ ,  $V_Z$  with respect to this frame of reference are obtained from the radial and transverse velocity components  $V_r$  and  $V_t$  by a standard transformation of vector components, similar to the one adopted in § 2.2 of Paper II. We note that because PSR J0737-3039 is located only 20 pc below the Galactic mid-plane [53], the unknown radial velocity  $V_r$  mainly affects the determination of  $V_X$  and  $V_Y$ .

As in Paper II, we calculate the motion of the system in the Galaxy backwards in time using the Galactic potential of Carlberg & Innanen [28] with updated model parameters derived by Kuijken & Gilmore [29] [54]. Since the present-day kinematical constraints only provide an upper limit of  $30\text{ km s}^{-1}$  on the transverse systemic velocity and the calculation of the past orbit requires precise starting values for both the present-day position and the present-day velocity, we calculate the motion backwards in time for two specific velocities:  $V_t = 10\text{ km s}^{-1}$  and  $V_t = 30\text{ km s}^{-1}$ . For each of these  $V_t$ , we integrate the equations of motion up to 100 Myr back in time for all possible  $V_r$ -values between  $-1500\text{ km s}^{-1}$  and  $1500\text{ km s}^{-1}$  (in steps of  $10\text{ km s}^{-1}$ ), and  $\Omega$ -values between  $0^\circ$  and  $360^\circ$  (in steps of  $5^\circ$ ). Although extremely high radial velocities in excess of  $\sim 1000\text{ km s}^{-1}$  may seem rather unlikely, they cannot be firmly excluded by the presently known observational constraints (see Paper II). The possibility of a high space velocity is also supported by observations of high-velocity single radio pulsars such as PSR B2224+65

(with  $V_t \gtrsim 800 \text{ km s}^{-1}$  [30]) and PSR B1508+55 (with  $V_t = 1083_{-90}^{+103} \text{ km s}^{-1}$  [31]). Moreover, as many of these high-velocity pulsars are expected to quickly escape the Galaxy, there is a strong bias against finding them. The fraction of radio pulsars formed with high space velocities is therefore not well constrained in the current pulsar sample.

In order to account for the possibility that PSR J0737-3039 has a large radial velocity and examine the effect of incorporating large radial velocities in the analysis, we weigh each considered radial velocity according to a pre-determined radial velocity distribution. For this purpose, we performed a population synthesis study of Galactic DNSs, including their kinematic evolution in the potential of Carlberg & Innanen [28]. Theoretical radial velocity distributions are then obtained by taking a snapshot of the population at the current epoch and determining the radial velocity for each DNS in the sample. The resulting PDFs are found to be represented well by Gaussian distributions with means of  $0 \text{ km s}^{-1}$  and velocity dispersions of  $60\text{--}200 \text{ km s}^{-1}$ , depending on the adopted population synthesis assumptions (see §IV B for more details). For comparison, we also consider a uniform radial velocity distribution in which all radial velocities between  $-1500 \text{ km s}^{-1}$  and  $1500 \text{ km s}^{-1}$  are equally probable [55]. It is clear that, contrary to what is stated by Piran & Shaviv [21], we do not assume the system to be moving almost exactly towards us with a very large radial velocity  $V_r$ . For the other unknown parameter, the orientation angle  $\Omega$  of the transverse velocity component in the plane perpendicular to the line-of-sight, we assume a uniform distribution between  $0^\circ$  and  $360^\circ$ .

As noted in the previous section, it is reasonable to assume that PSR J0737-3039 was born close to the Galactic plane, so that the intersections of the past orbits with the  $Z = 0$  plane yield possible birth sites as functions of  $V_r$  and  $\Omega$ . The number of Galactic plane crossings associated with each  $V_r$  and  $\Omega$ , within the adopted age limit of 100 Myr, can be anywhere between 1 and 5. The times in the past at which the system crosses the Galactic plane furthermore yield kinematic estimates for the age of the DNS, while subtraction of the Galactic rotational velocity from the total systemic velocity at the birth sites yields the peculiar velocity right after the formation of pulsar B.

Since the post-SN peculiar velocity represents one of the most important elements in constraining the kick velocity imparted to pulsar B at birth, it is worth taking a closer look at the range and distribution of the post-SN peculiar velocities derived from the Galactic motion calculations. In Fig. 1, the distribution of post-SN peculiar velocities is shown for a present-day transverse velocity component of  $30 \text{ km s}^{-1}$ , and kinematic age ranges of 0-100 Myr and 49-51 Myr. These probability distributions are calculated considering weights according to (i) the probability that the system has a present-day radial velocity  $V_r$  (assumed to be distributed according to a uniform or a Gaussian distribution), (ii) the transverse

velocity has a direction angle  $\Omega$  (assumed to be uniformly distributed), and (iii) the system is found at its current position in the Galaxy (determined by the time the system spends near its current position divided by its kinematic age, see §IV C for details). In particular, the probability that, for a given pair of  $V_r$  and  $\Omega$ , the post-SN peculiar velocity of the binary is equal to  $V_{\text{CM}}$  is given by

$$P(V_{\text{CM}}|V_r, \Omega) \propto \sum_{i=1}^{N(V_r, \Omega)} \frac{T(V_r, \Omega)}{\tau_{\text{kin},i}(V_r, \Omega)} \lambda_i(V_r, \Omega), \quad (1)$$

where  $N(V_r, \Omega)$  is the number of Galactic plane crossings associated with  $V_r$  and  $\Omega$ ,  $T(V_r, \Omega)$  is the time the system spends near its current position for the orbit associated with  $V_r$  and  $\Omega$ , and  $\tau_{\text{kin},i}(V_r, \Omega)$  is the kinematic age corresponding to the  $i$ -th plane crossing associated with  $V_r$  and  $\Omega$ . The factor  $\lambda_i(V_r, \Omega)$  is equal to 1 when the  $i$ -th plane crossing along the orbit associated with  $V_r$  and  $\Omega$  yields a post-SN peculiar velocity equal to  $V_{\text{CM}}$ , and equal to 0 otherwise. The total probability that the post-SN peculiar velocity of the binary is equal to  $V_{\text{CM}}$  is then obtained by integrating Eq. (1) over all possible values of  $V_r$  and  $\Omega$ :

$$P(V_{\text{CM}}) \propto \int_{\Omega} \int_{V_r} P(V_{\text{CM}}|V_r, \Omega) P(V_r) P(\Omega) dV_r d\Omega. \quad (2)$$

Here  $P(V_r)$  is the probability distribution of the unknown radial velocity  $V_r$ , and  $P(\Omega)$  the probability distribution of the unknown proper motion direction  $\Omega$  in the plane perpendicular to the line-of-sight.

For ages of 0-100 Myr, post-SN peculiar velocities up to  $100 \text{ km s}^{-1}$  are likely for all four radial velocity distributions. The highest post-SN peculiar velocities are found for the Gaussian radial velocity distributions with velocity dispersions of  $130 \text{ km s}^{-1}$  and  $200 \text{ km s}^{-1}$  ( $V_{\text{CM}}$  values remain likely up to  $200\text{--}300 \text{ km s}^{-1}$ ) and the uniform radial velocity distribution ( $V_{\text{CM}}$  values follow an almost flat distribution from  $300 \text{ km s}^{-1}$  to  $1500 \text{ km s}^{-1}$ ). For ages of 49-51 Myr, the post-SN peculiar velocity distributions all have a peak at  $50 \text{ km s}^{-1}$ . In the case of the uniform radial velocity distribution and the Gaussian distributions with velocity dispersions of  $130 \text{ km s}^{-1}$  or  $200 \text{ km s}^{-1}$ , additional peaks of almost equal height occur at even higher post-SN peculiar velocities. Similar conclusions apply to the post-SN peculiar velocity distributions obtained for a present-day transverse velocity component of  $10 \text{ km s}^{-1}$ . Despite the small lower limit on the present-day *transverse* systemic velocity, a wide range of non-negligible post-SN peculiar velocities is thus possible. We note however that the distributions incorporate all possible post-SN peculiar velocities obtained from tracing the motion of the system backwards in time and that some of these may require SN kicks and mass loss that are incompatible with the observational constraints on the orbital elements and component masses of the double pulsar.

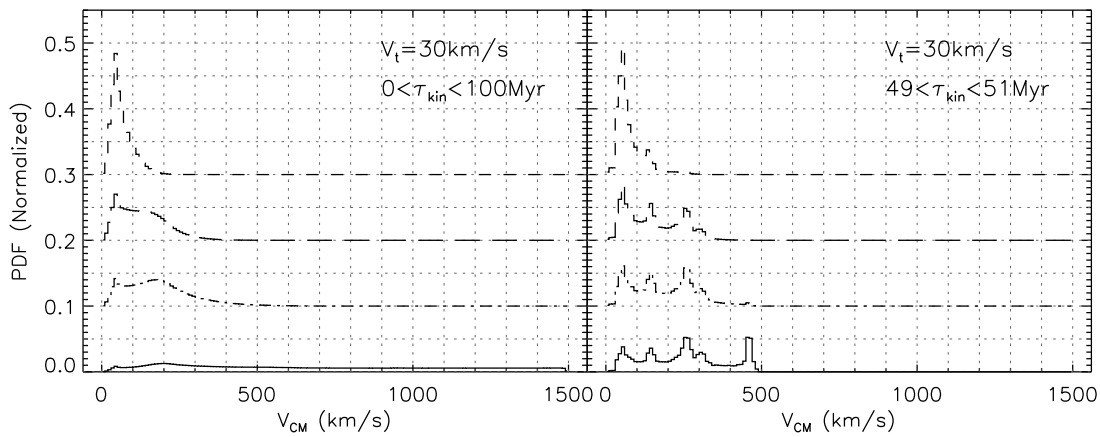


FIG. 1: Distribution of post-SN peculiar velocities for a present-day transverse velocity of  $30 \text{ km s}^{-1}$ , kinematic ages ranges of 0–100 Myr and 49–51 Myr, and radial velocity distributions varying from a uniform distribution (solid line) to Gaussian distributions with velocity dispersions of  $60 \text{ km s}^{-1}$  (long-dashed line),  $130 \text{ km s}^{-1}$  (short-dashed line), and  $200 \text{ km s}^{-1}$  (dash-dotted line). For clarity, the PDFs are offset from each other by an arbitrary amount.

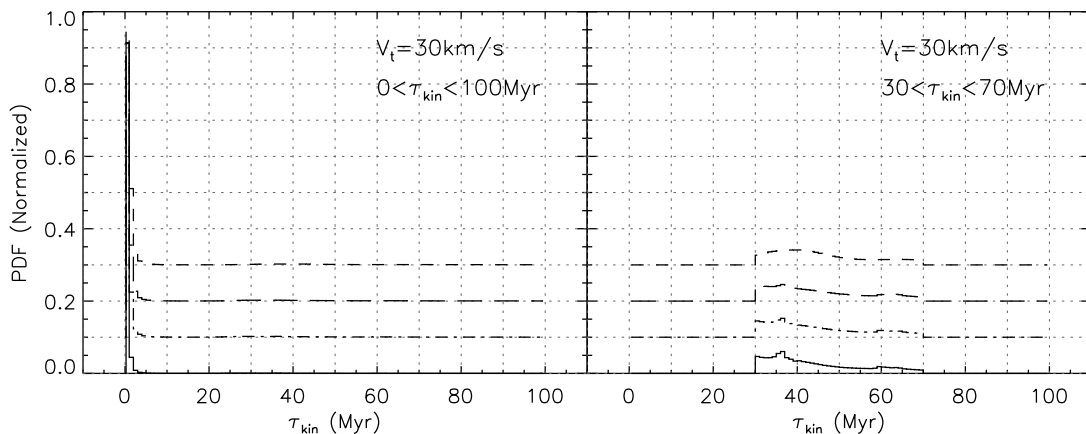


FIG. 2: Distribution of kinematic ages for a present-day transverse velocity of  $30 \text{ km s}^{-1}$ , kinematic age ranges of 0–100 Myr and 30–70 Myr, and radial velocity distributions varying from a uniform distribution (solid line) to Gaussian distributions with velocity dispersions of  $60 \text{ km s}^{-1}$  (long-dashed line),  $130 \text{ km s}^{-1}$  (short-dashed line), and  $200 \text{ km s}^{-1}$  (dash-dotted line). For clarity, the PDFs are offset from each other by an arbitrary amount.

Similarly, PDFs can be constructed for the kinematic ages  $\tau_{\text{kin}}$ . They are shown in Fig. 2 for a present-day transverse velocity component of  $30 \text{ km s}^{-1}$ , and kinematic age ranges of 0–100 Myr and 30–70 Myr. For ages of 0–100 Myr, the PDFs are all very strongly peaked at very young ages. In particular, 90–97% of the Galactic plane crossings give rise to ages of 0–5 Myr. The peak of the PDF at ages of 0–5 Myr furthermore increases with increasing velocity dispersion of the adopted radial velocity distribution. For ages of 30–70 Myr, the PDFs overall decrease with increasing values of  $\tau_{\text{kin}}$  and show no strong preference for any particular range of kinematic age values. Similar conclusions apply to the kinematic ages obtained for a present-day transverse velocity component of  $10 \text{ km s}^{-1}$ .

## B. Theoretical radial velocity distributions

While the radial velocity of PSR J0737-3039 is unknown, population synthesis calculations can provide us with some reasonable guidance on the expected radial velocity distribution of the DNS population. We use the *StarTrack* population synthesis code (see Belczynski et al. [9]; and especially Belczynski et al. [32] for an extensive and detailed description of this binary population synthesis evolutionary code) to develop models of DNS formation and evolution in our Galaxy (assuming continuous star-formation history over 10 Gyr and solar metallicity). To calculate the DNS kinematic evolution we need to also choose a spatial distribution of DNS binary progenitors in the Galaxy. We adopt a standard double exponential to represent the density distribution

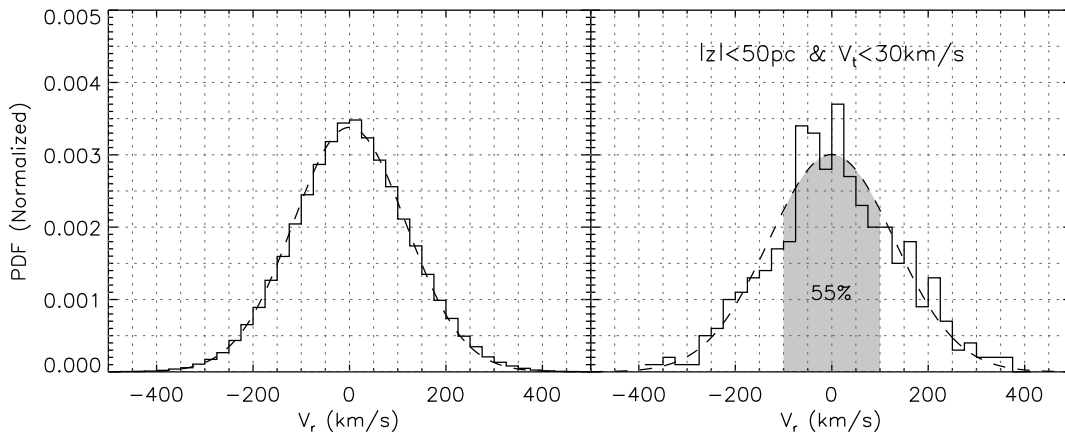


FIG. 3: Present-day radial-velocity distributions of coalescing DNSs for a population synthesis model with Maxwellian kicks with a velocity dispersion  $\sigma_{\text{kick}} = 250 \text{ km s}^{-1}$ . The left panel shows the distribution for the entire population of coalescing DNSs, while the right panel shows the distribution of coalescing DNSs within 50 pc of the Galactic mid-plane and with a proper motion of less than  $30 \text{ km s}^{-1}$ . The dashed lines in the left and right panels are best-fit Gaussian distributions with velocity dispersions of  $117 \text{ km s}^{-1}$  and  $130 \text{ km s}^{-1}$ , respectively. Note that in the right panel 45% of the systems have  $|V_r| > 100 \text{ km s}^{-1}$ .

TABLE II: Velocity Dispersions for Supernova Kicks and Radial Velocities

| $\sigma_{\text{kick}}^a$<br>( $\text{km s}^{-1}$ ) | $\sigma_{V_r}^b$<br>( $\text{km s}^{-1}$ ) |
|--|--|
| 50   | $63 \pm 2$                                 |
| 100  | $94 \pm 4$                                 |
| 150  | $92 \pm 4$                                 |
| 200  | $104 \pm 5$                                |
| 250  | $130 \pm 7$                                |
| 300  | $148 \pm 9$                                |
| 350  | $124 \pm 7$                                |
| 400  | $172 \pm 15$                               |
| 450  | $147 \pm 14$                               |
| 500  | $280 \pm 141$                              |

<sup>a</sup>Maxwellian distribution.

<sup>b</sup>Best fit Gaussian distribution centered at zero. Values are for coalescing DNSs within 50 pc of the Galactic mid-plane and with a proper motion of less than  $30 \text{ km s}^{-1}$ .

of Galactic systems:

$$n(R, z) = n_o \exp(-R/H_R) \exp(-|z|/H_Z), \quad (3)$$

where  $n_o = 1/(4\pi H_Z H_R^2)$  is the normalization,  $H_R$  the scale length, and  $H_Z$  the scale height. We adopt  $H_R = 2.8 \text{ kpc}$  and  $H_Z = 70 \text{ pc}$ , appropriate for massive stars. The motion of the DNSs in the Galaxy is calculated using the same Galactic potential as in §IV A.

In this analysis, we consider a set of models with input parameters chosen as for the standard model (model A) in Belczynski et al. [9], except for the assumed Maxwellian distributions of the kick magnitudes imparted to nascent neutron stars: we vary the one-dimensional kick velocity dispersion  $\sigma_{\text{kick}}$  in the range of  $50 - 500 \text{ km s}^{-1}$ , as shown in Table II. We restrict our parameter study to these models, because a broad

model exploration is not the primary goal of our study and because prior experience with DNS models clearly indicates that the assumed NS kick velocity model is the most important parameter affecting the DNS kinematic evolution and properties [12].

We use this set of DNS models to derive radial-velocity distributions with respect to the Sun. To obtain a realistic representation of the kinematic properties of the *current* population of tight DNS systems (like PSR J0737-3039), we place a cut on the model DNS populations and select only those that have already formed (i.e., they have a formation time shorter than 10 Gyr) and will coalesce within the age of the Universe (at a time in the range 9–14 Gyr). We next distribute the selected DNS population in the Galaxy and follow their motion using the calculated center-of-mass velocities imparted to the binaries after both of the two supernova events [56]. We also take into account the effect of Galactic rotation. We then derive the radial velocity distribution by extracting the calculated peculiar velocities (relative to the Sun) and considering the appropriate projections. We can further impose a number of additional constraints on the model population to select systems that have kinematic properties similar to PSR J0737-3039: coalescing DNS with proper motion smaller than  $30 \text{ km s}^{-1}$  and a location within 50 pc from the Galactic plane; we note that we do not impose any constraints on the binary properties to avoid any statistical accuracy problems.

We find that the derived radial velocity distributions are very well approximated by a Gaussian centered at zero with velocity dispersions  $\sigma_{V_r}$  ranging from 60 to  $200 \text{ km s}^{-1}$ . The dependence of the derived radial-velocity dispersions on the kick velocity dispersions are shown in Table II. The distributions with and without the kinematic constraints are shown in Figure 3, for  $\sigma_{\text{kick}} = 250 \text{ km s}^{-1}$ . The corresponding values of  $\sigma_{V_r}$

for the two panels are rather similar:  $117 \text{ km s}^{-1}$  and  $130 \text{ km s}^{-1}$ , respectively. Moreover, for this  $\sigma_{\text{kick}}$  value, 45% of the systems have  $|V_r| > 100 \text{ km s}^{-1}$ .

It is important to note that imposing the proper-motion constraint does not actually reduce the typical magnitude of the radial velocity. The reason is that small proper motion values select two sub-populations of DNS systems: one with inherently small center-of-mass velocities (and consequently small radial velocities), and another with large center-of-mass velocities but appropriate direction so that the proper motion is small. This second group naturally leads to large radial velocities because, for a given center-of-mass velocity, the projection affects the radial component in the opposite way as it does the transverse component. Piran & Shaviv [21] somewhat misleadingly draw the focus away from this second group and use the first sub-population to argue that both the present *and* post-SN peculiar velocity must be small. Since our theoretical radial-velocity distributions incorporate the constraints  $|Z| < 50 \text{ pc}$  and  $V_t < 30 \text{ km s}^{-1}$ , they implicitly account for the geometrical probability argument by Piran & Shaviv [21] that the probability of a small transverse velocity component is larger for smaller total systemic peculiar velocities (see their Eq. 2). Moreover, as outlined in detail in the previous section, we explicitly account for differences between the system's current and post-SN peculiar velocity by modeling its past motion in the Galactic potential.

Last, we note (although not directly relevant to this study) that with the full population synthesis models we confirm the results of Kalogera et al. [33] about the vertical DNS distribution: for  $\sigma_{\text{kick}} = 250 \text{ km s}^{-1}$ , it is best fitted by two exponentials, each with a typical scale height of  $0.230 \pm 0.006 \text{ kpc}$  and  $1.72 \pm 0.07 \text{ kpc}$ . As expected the scale height increases with increasing typical kick magnitude.

### C. Probability to find the system at its current position

At a distance of  $\sim 600 \text{ pc}$  and a Galactic latitude of  $-4.5^\circ$ , PSR J0737-3039 is currently located only  $20 \text{ pc}$  below the Galactic plane. Piran & Shaviv [19] used the proximity of the system to the Galactic plane to argue that pulsar B most likely received only a small kick velocity at birth and that its helium star progenitor most likely had a pre-SN mass only slightly larger than the pulsar's present mass. Their procedure, however, only accounted for the motion of the system perpendicular to the Galactic plane.

Here, we determine the probability of finding the system at its current position in the Galaxy in three dimensions (i.e., besides the vertical distance to the Galactic plane, we also consider the radial and azimuthal position in the plane). For this purpose, we determine the time the system spends in a sphere with radius  $R$  centered on its current location for all  $V_r$ - and  $\Omega$ -values considered

for the derivation of the possible birth sites in §IV A. The probability to find the system near its current position is then determined as the time it spends in this sphere divided by its age. For the latter, we adopt the kinematic ages obtained by tracing the motion of the system backwards in time, so that the probability of finding the system near its current position depends on the radial velocity  $V_r$ , the proper motion direction  $\Omega$ , and the Galactic plane crossing considered along the orbit associated with  $V_r$  and  $\Omega$ . We performed some test calculations to successfully verify that the results based on the thus determined probabilities are insensitive to the adopted value of  $R$ , as long as it is sufficiently small for the sphere to represent a local neighborhood near the system's current position. For the results presented in this paper we, somewhat arbitrarily, choose  $R = 50 \text{ pc}$ .

## V. PROGENITOR CONSTRAINTS

### A. Post-supernova orbital parameters

After the formation of pulsar B, the evolution of the system is expected to be driven exclusively by the emission of gravitational waves. The post-SN orbital semi-major axis and eccentricity can then be obtained from the current values by numerically integrating the system of differential equations governing the orbital evolution due to gravitational wave emission backwards in time. For this purpose, we use the differential equations derived by Junker & Schäfer [34] which are valid up to 3.5 post-Newtonian order of approximation.

We calculate the orbital evolution backwards in time for all Galactic plane crossings associated with all values of  $V_r$  and  $\Omega$  considered in the calculation of the possible birth sites. For each crossing the integration is terminated at the associated kinematic age  $\tau_{\text{kin}}$ . We find the resulting post-SN orbital separation  $A$  to be always between  $1.26 R_\odot$  and  $1.54 R_\odot$ , and the post-SN orbital eccentricity  $e$  between 0.088 and 0.12 (see Papers I and II). Since the kinematic ages are functions of the radial velocity  $V_r$ , the proper motion direction  $\Omega$ , and the Galactic plane crossing considered along the past orbit associated with  $V_r$  and  $\Omega$ , the particular values of  $A$  and  $e$  associated with a given  $\tau_{\text{kin}}$  are also functions of these variables.

### B. Orbital dynamics of asymmetric supernova explosions

The pre- and post-SN binary parameters and the kick velocity imparted to pulsar B at birth are related by the conservation laws of orbital energy and angular momentum. For a circular pre-SN orbit, the relations take the



form [e.g. 35–37, 37–39]

$$\begin{aligned} & V_k^2 + V_0^2 + 2 V_k V_0 \cos \theta \\ &= G (M_A + M_B) \left( \frac{2}{A_0} - \frac{1}{A} \right), \end{aligned} \quad (4)$$

$$\begin{aligned} & A_0^2 [V_k^2 \sin^2 \theta \cos^2 \phi + (V_k \cos \theta + V_0)^2] \\ &= G (M_A + M_B) A (1 - e^2), \end{aligned} \quad (5)$$

where  $M_0$  is the mass of pulsar B’s pre-SN helium star progenitor,  $A_0$  the pre-SN orbital separation,  $V_0 = [G(M_A + M_0)/A_0]^{1/2}$  the relative orbital velocity of pulsar B’s pre-SN helium star progenitor, and  $V_k$  the magnitude of the kick velocity imparted to pulsar B at birth. The angles  $\theta$  and  $\phi$  define the direction of the kick velocity imparted to pulsar B:  $\theta$  is the polar angle between  $\vec{V}_k$  and  $\vec{V}_0$ , and  $\phi$  the corresponding azimuthal angle in the plane perpendicular to  $\vec{V}_0$  defined so that  $\phi = \pi/2$  corresponds to the direction from pulsar A to pulsar B’s helium star progenitor (see Fig. 1 in [22] for a graphical representation).

The requirement that Eqs. (4) and (5) permit real solutions for  $V_k$ ,  $\theta$ ,  $\phi$ ,  $M_0$ , and  $A_0$ , imposes constraints on the pre- and post-SN binary parameters and on the magnitude and direction of the kick velocity imparted to pulsar B at birth. For a mathematical formulation of these constraints, we refer to Eqs. (21)–(27) in [40], and references therein (a more compact description can also be found in Papers I and II). We here merely recall that the constraints express that: (i) the binary components must remain bound after the SN explosion, (ii) the pre- and post-SN orbits must pass through the instantaneous position of the component stars at the time of the SN explosion, and (iii) there is a lower and upper limit on the degree of orbital contraction or expansion associated with a given amount of mass loss and a given SN kick.

Besides the changes in the orbital parameters and the mass of the exploding star, the SN explosion also imparts a kick velocity to the binary’s center of mass and tilts the post-SN orbital plane with respect to the pre-SN one. Under the assumption that the pre-SN peculiar velocity of the binary is small in comparison to the pre-SN orbital velocity of the component stars, the magnitude of the post-SN center-of-mass velocity  $V_{\text{CM}}$  is given by [e.g. 37]

$$\begin{aligned} V_{\text{CM}}^2 &= \frac{M_B M_0}{(M_A + M_0)(M_A + M_B)} \left[ \frac{G(M_0 - M_B)M_A}{M_0 A} \right. \\ &\quad \left. + \frac{G(M_0 - M_B)(M_0 - 2M_B)M_A}{M_0 M_B A_0} + V_k^2 \right]. \end{aligned} \quad (6)$$

The tilt angle  $\lambda$  between the pre- and post-SN orbital planes is given by [22]

$$\begin{aligned} \cos \lambda &= \left[ \frac{A}{A_0} \frac{M_A + M_B}{M_A + M_0} (1 - e^2) \right]^{-1/2} \\ &\quad \times \left( \frac{V_k}{V_0} \cos \theta + 1 \right). \end{aligned} \quad (7)$$

From Eqs. (5) and (7), one derives that  $\lambda = 0^\circ$  for kicks directed in the pre-SN orbital plane (i.e.  $\cos \theta = \pm 1$ ), independent of the kick velocity magnitude  $V_k$ .

### C. Stellar and binary evolution

The constraints on the progenitor of PSR J0737-3039 resulting from the dynamics of asymmetric SN explosions arise solely from tracing the evolution of the current system properties backwards in time. The pre-SN orbital separations and pulsar B progenitor masses found this way are, however, not necessarily accessible through the currently known DNS formation channels. Further constraints on the progenitor of pulsar B can therefore be obtained from stellar and binary evolution calculations.

A lower limit on the mass of pulsar B’s pre-SN progenitor is given by the requirement that the star must be massive enough to evolve into a NS rather than a white dwarf. According to our current understanding of helium star evolution, the minimum helium star mass required for NS formation is  $2.1\text{--}2.8 M_\odot$  [10, 41]. The actual helium star minimum mass is, however, still considerably uncertain due to the poorly understood evolution of massive stars and possible interactions with close binary companions.

As in Papers I and II, we impose a lower limit of  $2.1 M_\odot$  on the mass of pulsar B’s pre-SN helium star progenitor. However, in the light of recent suggestions that the progenitor of pulsar B may have been significantly less massive than the conventional lower limit of  $2.1 M_\odot$ , we also explore the possibility of progenitor masses as low as pulsar B’s present-day mass of  $1.25 M_\odot$  [3, 19]. Unless our current understanding of helium star evolution is seriously flawed, this scenario implies that the progenitor of pulsar B must have lost a significant amount of mass (at least  $\sim 0.7 M_\odot$ ) after it had already established a sufficiently massive core to guarantee the occurrence of a future SN explosion. We note that this possibility is included in the binary population synthesis calculations used to derive the adopted theoretical DNS radial-velocity distributions (see Table II). Contrary to what is stated by Piran & Shaviv [21], our population synthesis calculations do allow for low-mass helium-rich progenitors of the second NS and the derived radial-velocity distributions are therefore by no means a priori biased towards high progenitor masses.

In Paper I, we also showed that the pre-SN binary was so tight ( $1.2 R_\odot \lesssim A_0 \lesssim 1.7 R_\odot$ ) that the helium star progenitor of pulsar B must have been overflowing its Roche lobe at the time of its SN explosion (see also [13]). An upper limit on the progenitor mass is therefore given by the requirement that this mass-transfer phase be dynamically stable (otherwise the components would have merged and no DNS would have formed)[57]. Based on the evolutionary tracks for NS + helium star binaries calculated by Ivanova et al. [42], we adopt an upper limit of 3.5 on the mass ratio  $M_0/M_A$  of the pre-

SN binary to separate dynamically stable from dynamically unstable Roche-lobe overflow (see also [43, 44]). For  $M_A = 1.34 M_\odot$ , this yields an upper limit of  $4.7 M_\odot$  on the mass of pulsar B’s pre-SN helium star progenitor. Because of the mass transfer, the pre-SN progenitor mass may, however, be considerably lower than the progenitor mass at the onset of Roche-lobe overflow. The upper limit of  $4.7 M_\odot$  is therefore fairly conservative. However, as we will see in the next section, the preferred pre-SN progenitor masses are always significantly smaller than  $4.7 M_\odot$  so that a stricter upper limit would not considerably affect any of our results.

## VI. PROBABILITY DISTRIBUTION FUNCTIONS

### A. A coherent picture for the progenitor and formation of pulsar B

The steps outlined in the previous sections have been used to derive the most likely pre-SN progenitor of PSR J0737-3039 and the magnitude and direction of the kick velocity imparted to pulsar B at birth. Firstly, the possible kinematic ages and post-SN peculiar velocities are determined by tracing the Galactic motion backwards in time using the current constraints on the proper motion and position in the Galaxy. These ages and velocities are functions of the presently unknown values of the radial velocity  $V_r$  and proper motion direction  $\Omega$ . Secondly, the kinematic ages are used to reverse the orbital evolution due to gravitational radiation and determine the orbital semi-major axis and eccentricity right after the formation of pulsar B. Thirdly, the pre-SN binary parameters and kick velocity imparted to pulsar B are constrained using the conservation of orbital energy and angular momentum during asymmetric SN explosions. The constraints are supplemented with the requirements that the post-SN peculiar velocity obtained from Eq. (6) be compatible with the post-SN peculiar velocity obtained by tracing the motion of the system in the Galaxy backwards in time, and that the spin-orbit misalignment of pulsar A obtained from Eq. (7) be compatible with the observational constraint  $|\lambda - 90^\circ| > 30^\circ$ . Imposing the latter constraint rests on the additional assumption that pulsar A’s spin is aligned with the pre-SN orbital angular momentum, as expected from the strong tidal interactions operating during the spin-up phase of pulsar A.

### B. The most likely kick velocity and progenitor properties

Since the conservation laws of orbital energy and angular momentum yield two equations for five unknown quantities  $V_k$ ,  $\cos\theta$ ,  $\phi$ ,  $M_0$ , and  $A_0$ , we solve the equations for  $M_0$  and  $A_0$  as functions of  $V_k$ ,  $\cos\theta$ , and  $\phi$ . Each solution is then weighted assuming uniform prior

TABLE III: Effect of marginalizing the 5-D PDF for  $V_k$ ,  $\cos\theta$ ,  $\phi$ ,  $M_0$ , and  $A_0$  on the most likely kick velocity and progenitor parameters for a transverse velocity component of  $30 \text{ km s}^{-1}$ , a minimum helium star mass of  $1.25 M_\odot$ , an age range of 0–100 Myr, and a uniform present-day radial velocity distribution.

| Variables                         | Most likely value               |              |                 |                        |                        |
|-----------------------------------|---------------------------------|--------------|-----------------|------------------------|------------------------|
|                                   | $V_k$<br>( $\text{km s}^{-1}$ ) | $\cos\theta$ | $\phi$<br>(deg) | $M_0$<br>( $M_\odot$ ) | $A_0$<br>( $R_\odot$ ) |
| $V_k, \cos\theta, \phi, M_0, A_0$ | 75                              | -0.025       | 10              | 1.45                   | 1.15                   |
| $V_k, \cos\theta, \phi, M_0$      | 75                              | -0.025       | 10              | 1.45                   |                        |
| $V_k, \cos\theta, M_0$            | 45                              | -0.050       |                 | 1.45                   |                        |
| $V_k, M_0$                        | 10                              |              |                 | 1.45                   |                        |
| $V_k$                             | 55                              |              |                 |                        |                        |

distributions for  $V_k$ ,  $\cos\theta$ ,  $\phi$ ,  $M_0$ , and  $A_0$ . Thus the kick direction is assumed to be isotropically distributed in space. Similar to Eqs. (1) and (2), we next determine the probability that, given the currently known observational constraints, PSR J0737-3039B was born with a natal kick velocity  $V_k$  with a direction determined by  $\cos\theta$  and  $\phi$  from a progenitor of mass  $M_0$  orbiting the first-born pulsar in a circular orbit of radius  $A_0$  as

$$\begin{aligned}
 & P(V_k, \cos\theta, \phi, M_0, A_0 | X_{\text{obs}}) \\
 & \propto \int_{\Omega} \int_{V_r} \left[ \sum_{i=1}^{N(V_r, \Omega)} \frac{T(V_r, \Omega)}{\tau_{\text{kin}, i}(V_r, \Omega)} \kappa_i(V_r, \Omega) \right] \quad (8) \\
 & \times P(V_r) P(\Omega) dV_r d\Omega.
 \end{aligned}$$

Here  $X_{\text{obs}}$  denotes all currently known observational constraints (orbital separation, eccentricity, proper motion, etc). The factor  $\kappa_i(V_r, \Omega)$  is equal to 1 when the considered  $V_k$ ,  $\cos\theta$ ,  $\phi$ ,  $M_0$ , and  $A_0$  satisfy all constraints imposed by tracing the system’s kinematic and evolutionary history back to the formation time of pulsar B for the  $i$ -th plane crossing along the orbit in the Galaxy associated with  $V_r$  and  $\Omega$ , and equal to 0 otherwise. The other quantities are defined in §IV A. Hence, we obtain a 5-dimensional PDF for the kick velocity and progenitor parameters:  $V_k$ ,  $\cos\theta$ ,  $\phi$ ,  $M_0$ , and  $A_0$ .

The construction of the full 5-D PDF represents a significant departure from previous investigations which restricted the analysis to the derivation of 1-D PDFs for  $V_k$  (Papers I and II) or 2-D PDFs for  $V_k$  and  $M_0$  [19, 20]. Although the derivation of the most likely  $V_k$  and  $M_0$  values from these marginalized PDFs is mathematically correct, they may be subjected to projection effects which can drastically affect the position of the maxima. In order to illustrate this, we constructed the 5-D PDF for a transverse velocity component of  $30 \text{ km s}^{-1}$ , a minimum helium star mass of  $1.25 M_\odot$ , an age range of 0–100 Myr, and a uniform present-day radial velocity distribution. The most likely kick velocity and progenitor properties obtained from the 5-D PDF are  $V_k \simeq 75 \text{ km s}^{-1}$ ,  $\cos\theta \simeq -0.025$ ,  $\phi = 10^\circ$ ,  $M_0 \simeq 1.45 M_\odot$ , and  $A_0 \simeq 1.15 R_\odot$ . The most likely values obtained af-

ter successively integrating over  $A_0$ ,  $\phi$ ,  $\cos\theta$ , and  $M_0$  are listed in Table III. While the integration over  $A_0$  does not significantly affect the most likely value of  $V_k$ , successive integrations over  $\phi$  and  $\cos\theta$  reduce the most likely  $V_k$  to  $45 \text{ km s}^{-1}$  and  $10 \text{ km s}^{-1}$ , respectively. A subsequent integration over  $M_0$  furthermore increases the most likely  $V_k$  back to  $55 \text{ km s}^{-1}$ . Marginalizing a multi-dimensional PDF can thus have a significant impact on the location of its peaks. Some caution is therefore in order when interpreting marginalized PDFs.

The most likely kick velocity and progenitor parameters can also depend strongly on the assumptions underlying the reconstruction of the binary’s evolutionary history (i.e., the magnitude of the transverse systemic velocity component, the minimum helium star mass required for the formation of a NS, the age of the system, and the probability distribution of the unknown radial velocity). In order to investigate this, we systematically calculated the 5-D PDFs for  $V_k$ ,  $\cos\theta$ ,  $\phi$ ,  $M_0$ , and  $A_0$  for different sets of prior assumptions. The resulting most likely kick velocity and progenitor parameters are summarized in Table IV. The dependence of the most likely  $V_k$ ,  $\cos\theta$ , and  $M_0$  on the adopted prior assumptions is also presented graphically in Figs. 4–6. For brevity, we denote the uniform radial velocity distribution in the table and figures as a Gaussian distribution with an infinite radial velocity dispersion.

The most likely kick velocity imparted to pulsar B at birth is smaller than  $50 \text{ km s}^{-1}$  only when the transverse velocity component has a magnitude of  $10 \text{ km s}^{-1}$ , the minimum helium star mass required for NS formation is allowed to be as low as  $1.25 M_\odot$ , and the age of the system is assumed to be between 30 and 70 Myr. *All other models* yield most likely kick velocities of  $50\text{--}180 \text{ km s}^{-1}$ . When a minimum pre-SN helium star mass of  $2.1 M_\odot$  is imposed, the kicks are always strongly favored to be directed opposite to the helium star’s pre-SN orbital motion (most likely  $\cos\theta \simeq -0.90 \pm 0.05$ ). When the constraint on the minimum pre-SN helium star mass is relaxed, the most likely kick direction can shift significantly and can even become perpendicular to the helium star’s pre-SN orbital velocity. Allowing pre-SN helium star masses down to  $1.25 M_\odot$  furthermore always leads to most likely progenitor masses of  $1.3\text{--}2.0 M_\odot$ , *except* when  $V_i = 10 \text{ km s}^{-1}$ , the age of the system is between 0 and 100 Myr, and the radial velocities are distributed uniformly or according to a Gaussian with a velocity dispersion of  $200 \text{ km s}^{-1}$ .

In summary, while small kick velocities of just a few tens of  $\text{km s}^{-1}$  could be favored for some models, the majority of the models yields most likely values of  $50\text{--}180 \text{ km s}^{-1}$ . Progenitor masses below  $2.1 M_\odot$  are furthermore not required to explain the system properties, although they are generally favored when helium stars below  $2.1 M_\odot$  are still assumed to be viable NS progenitors. We note though that the results presented in Table IV and the associated figures are based on the assumption that all kick velocity magnitudes  $V_k$  are equally probable. This assumption is inconsistent for models using the

Gaussian radial velocity distributions based on population synthesis calculations of coalescing DNSs. In particular, these calculations all adopt a Maxwellian rather than a uniform kick velocity distribution. In all cases, weighing the kick velocities according to the Maxwellian underlying the derivation of the radial velocity distributions would, however, shift the most likely kick velocities to higher  $V_k$  values than listed in Table IV. This reinforces our conclusion that the presently known observational constraints not necessarily disfavor kick velocity magnitudes of  $100 \text{ km s}^{-1}$  or more.

### C. Confidence limits on the kick velocity and progenitor parameters

The use of the full 5-D PDF for  $V_k$ ,  $\cos\theta$ ,  $\phi$ ,  $M_0$ , and  $A_0$  in the derivation of the most likely pulsar B kick velocity and progenitor parameters has the advantage of being free of projection effects, but is much more cumbersome and computationally expensive for the calculation of confidence limits. Since our main aim in this paper is to present a differential analysis showing the effects of different model assumptions, we adopt a simpler approach and determine the confidence limits from marginalized 1-D PDFs. We recognize, however, that in doing so, projection effects may play a significant role and any information on possible correlations between the different parameters will be lost.

For illustration, some representative 1-D PDFs used for the calculation of the confidence limits in the case of a present-day transverse velocity component of  $10 \text{ km s}^{-1}$  are shown in Fig. 7. Panels (a)–(c) show the kick velocity distributions resulting from different present-day radial velocity distributions for ages ranges of 0–100 Myr and 49–51 Myr, and minimum pre-SN helium star masses of  $1.25 M_\odot$  and  $2.1 M_\odot$ . For a given age range and minimum pre-SN helium star mass, the PDFs show a peak which is most pronounced when a Gaussian radial velocity distribution with a velocity dispersion of  $60 \text{ km s}^{-1}$  is considered, and which widens with increasing radial velocity dispersions. When the age is assumed to be 0–100 Myr and the minimum pre-SN helium star mass  $1.25 M_\odot$ , there is a clear tendency for the 1-D PDFs to favor kick velocities of  $50 \text{ km s}^{-1}$  or less (although this becomes significantly less pronounced with increasing radial velocity dispersions). This trend shifts towards favoring kick velocities of  $50\text{--}100 \text{ km s}^{-1}$  when the age range is narrowed to 49–51 Myr. Moreover, when the age range is kept fixed at 0–100 Myr, but the minimum pre-SN helium star mass is increased to  $2.1 M_\odot$ , the favored range of kick velocities shifts to  $100\text{--}150 \text{ km s}^{-1}$ . In the latter case, the kick velocity is furthermore always required to be larger than  $\sim 60 \text{ km s}^{-1}$  (see also Papers I and II).

In Panels (d)–(e), we show the distribution of  $\cos\theta$  for different present-day radial velocity distributions, DNS ages of 0–100 Myr, and minimum pre-SN helium star masses of  $1.25 M_\odot$  and  $2.1 M_\odot$ . For a minimum he-

TABLE IV: The most likely kick velocity and progenitor parameters obtained from the 5-D PDF for  $V_k$ ,  $\cos\theta$ ,  $\phi$ ,  $M_0$ , and  $A_0$ , for different transverse systemic velocity components, minimum pre-SN helium star masses, DNS ages, and present-day radial velocity distributions. For brevity, the uniform radial velocity distribution is denoted by  $\sigma_{V_r} = \infty$ . Tabulated values of  $\phi$  are restricted to  $0^\circ \leq \phi \leq 90^\circ$ . For each listed  $\phi$ -value additional and equally likely solutions to Eqs. (4) and (5) are associated with  $-\phi$  and  $180^\circ \pm \phi$ . For  $V_k$  and  $M_0$ , 68% and 90% confidence intervals are also listed. The intervals are obtained by marginalizing the 5-D PDF to 1-D PDFs for  $V_k$  and  $M_0$ .

| Priors                          |                                     |                              |  | Most likely progenitor          |                       |                 |                        |                        | 68% confidence intervals        |                        | 90% confidence intervals        |                        |
|---------------------------------|-------------------------------------|------------------------------|--|---------------------------------|-----------------------|-----------------|------------------------|------------------------|---------------------------------|------------------------|---------------------------------|------------------------|
| $V_t$<br>( $\text{km s}^{-1}$ ) | $M_{0,\text{min}}$<br>( $M_\odot$ ) | $\tau_{\text{kin}}$<br>(Myr) | $\sigma_{V_r}$<br>( $\text{km s}^{-1}$ ) | $V_k$<br>( $\text{km s}^{-1}$ ) | $\cos\theta$<br>(deg) | $\phi$<br>(deg) | $M_0$<br>( $M_\odot$ ) | $A_0$<br>( $R_\odot$ ) | $V_k$<br>( $\text{km s}^{-1}$ ) | $M_0$<br>( $M_\odot$ ) | $V_k$<br>( $\text{km s}^{-1}$ ) | $M_0$<br>( $M_\odot$ ) |
| 10                              | 2.1                                 | 0-100                        | $\infty$                                 | 170                             | -0.925                | 45              | 2.65                   | 1.35                   | 105-335                         | 2.1-3.3                | 75-535                          | 2.1-4.2                |
| 10                              | 2.1                                 | 0-100                        | 200                                      | 160                             | -0.925                | 45              | 2.55                   | 1.35                   | 95-255                          | 2.1-2.8                | 75-345                          | 2.1-3.5                |
| 10                              | 2.1                                 | 0-100                        | 130                                      | 125                             | -0.900                | 65              | 2.25                   | 1.35                   | 95-215                          | 2.1-2.6                | 75-285                          | 2.1-3.1                |
| 10                              | 2.1                                 | 0-100                        | 60                                       | 80                              | -0.950                | 15              | 2.15                   | 1.15                   | 75-155                          | 2.1-2.4                | 65-195                          | 2.1-2.6                |
| 10                              | 2.1                                 | 30-70                        | $\infty$                                 | 120                             | -0.875                | 75              | 2.25                   | 1.45                   | 95-285                          | 2.1-3.1                | 75-405                          | 2.1-3.9                |
| 10                              | 2.1                                 | 30-70                        | 200                                      | 120                             | -0.875                | 80              | 2.25                   | 1.45                   | 95-255                          | 2.1-2.9                | 65-345                          | 2.1-3.6                |
| 10                              | 2.1                                 | 30-70                        | 130                                      | 120                             | -0.875                | 80              | 2.25                   | 1.45                   | 85-225                          | 2.1-2.7                | 65-305                          | 2.1-3.3                |
| 10                              | 2.1                                 | 30-70                        | 60                                       | 75                              | -0.950                | 15              | 2.15                   | 1.25                   | 75-155                          | 2.1-2.4                | 65-205                          | 2.1-2.6                |
| 10                              | 2.1                                 | 49-51                        | $\infty$                                 | 70                              | -0.950                | 15              | 2.15                   | 1.25                   | 65-105, 165-355                 | 2.1-2.3, 2.7-3.8       | 65-455                          | 2.1-4.1                |
| 10                              | 2.1                                 | 49-51                        | 200                                      | 70                              | -0.950                | 15              | 2.15                   | 1.25                   | 65-125, 165-315                 | 2.1-2.4, 2.7-3.6       | 65-395                          | 2.1-3.8                |
| 10                              | 2.1                                 | 49-51                        | 130                                      | 70                              | -0.950                | 15              | 2.15                   | 1.25                   | 65-135, 165-265                 | 2.1-2.4, 2.8-3.3       | 65-345                          | 2.1-3.3, 3.5-3.7       |
| 10                              | 2.1                                 | 49-51                        | 60                                       | 70                              | -0.950                | 15              | 2.15                   | 1.25                   | 65-125                          | 2.1-2.3                | 65-215                          | 2.1-2.8                |
| 10                              | 1.25                                | 0-100                        | $\infty$                                 | 170                             | -0.925                | 45              | 2.65                   | 1.35                   | 0-275                           | 1.3-2.8                | 0-475                           | 1.25-3.8               |
| 10                              | 1.25                                | 0-100                        | 200                                      | 160                             | -0.925                | 45              | 2.55                   | 1.35                   | 0-185                           | 1.3-2.3                | 0-305                           | 1.25-2.9               |
| 10                              | 1.25                                | 0-100                        | 130                                      | 50                              | -0.050                | 75              | 1.35                   | 1.25                   | 0-135                           | 1.25-1.9               | 0-235                           | 1.25-2.5               |
| 10                              | 1.25                                | 0-100                        | 60                                       | 50                              | -0.050                | 75              | 1.35                   | 1.25                   | 0-65                            | 1.3-1.6                | 0-115                           | 1.25-1.8               |
| 10                              | 1.25                                | 30-70                        | $\infty$                                 | 5                               | -0.200                | 20              | 1.55                   | 1.25                   | 0-145                           | 1.25-2.0               | 0-295                           | 1.25-3.0               |
| 10                              | 1.25                                | 30-70                        | 200                                      | 5                               | -0.175                | 15              | 1.55                   | 1.25                   | 0-115                           | 1.25-1.8               | 0-235                           | 1.25-2.6               |
| 10                              | 1.25                                | 30-70                        | 130                                      | 5                               | -0.175                | 15              | 1.55                   | 1.25                   | 0-95                            | 1.25-1.7               | 0-195                           | 1.25-2.3               |
| 10                              | 1.25                                | 30-70                        | 60                                       | 5                               | -0.175                | 15              | 1.55                   | 1.25                   | 0-65                            | 1.3-1.6                | 0-105                           | 1.25-1.8               |
| 10                              | 1.25                                | 49-51                        | $\infty$                                 | 95                              | -0.775                | 80              | 1.95                   | 1.45                   | 0-155                           | 1.3-2.0                | 0-285                           | 1.25-2.2, 2.8-3.7      |
| 10                              | 1.25                                | 49-51                        | 200                                      | 95                              | -0.775                | 80              | 1.95                   | 1.45                   | 0-145                           | 1.4-2.0                | 0-225                           | 1.25-2.2, 3.1-3.2      |
| 10                              | 1.25                                | 49-51                        | 130                                      | 90                              | -0.750                | 80              | 1.85                   | 1.45                   | 0-125                           | 1.4-2.0                | 0-195                           | 1.25-2.1               |
| 10                              | 1.25                                | 49-51                        | 60                                       | 85                              | -0.725                | 80              | 1.85                   | 1.45                   | 0-95                            | 1.3-1.9                | 0-155                           | 1.25-2.0               |
| 30                              | 2.1                                 | 0-100                        | $\infty$                                 | 130                             | -0.925                | 70              | 2.35                   | 1.25                   | 105-315                         | 2.1-3.2                | 75-485                          | 2.1-4.1                |
| 30                              | 2.1                                 | 0-100                        | 200                                      | 120                             | -0.900                | 65              | 2.25                   | 1.25                   | 95-235                          | 2.1-2.7                | 75-325                          | 2.1-3.3                |
| 30                              | 2.1                                 | 0-100                        | 130                                      | 120                             | -0.900                | 65              | 2.25                   | 1.25                   | 85-195                          | 2.1-2.6                | 75-275                          | 2.1-3.0                |
| 30                              | 2.1                                 | 0-100                        | 60                                       | 80                              | -0.950                | 15              | 2.15                   | 1.15                   | 75-145                          | 2.1-2.3                | 75-195                          | 2.1-2.5                |
| 30                              | 2.1                                 | 30-70                        | $\infty$                                 | 140                             | -0.950                | 15              | 2.75                   | 1.25                   | 105-285                         | 2.1-3.1                | 75-405                          | 2.1-3.9                |
| 30                              | 2.1                                 | 30-70                        | 200                                      | 140                             | -0.950                | 15              | 2.75                   | 1.25                   | 95-255                          | 2.1-2.9                | 75-355                          | 2.1-3.6                |
| 30                              | 2.1                                 | 30-70                        | 130                                      | 120                             | -0.875                | 75              | 2.25                   | 1.45                   | 85-225                          | 2.1-2.8                | 65-315                          | 2.1-3.3                |
| 30                              | 2.1                                 | 30-70                        | 60                                       | 75                              | -0.950                | 15              | 2.15                   | 1.25                   | 75-165                          | 2.1-2.4                | 65-215                          | 2.1-2.7                |
| 30                              | 2.1                                 | 49-51                        | $\infty$                                 | 175                             | -0.950                | 15              | 3.15                   | 1.25                   | 85-285                          | 2.1-3.2                | 65-405                          | 2.1-3.8                |
| 30                              | 2.1                                 | 49-51                        | 200                                      | 120                             | -0.925                | 75              | 2.15                   | 1.55                   | 85-255                          | 2.1-3.1                | 65-345                          | 2.1-3.6                |
| 30                              | 2.1                                 | 49-51                        | 130                                      | 120                             | -0.925                | 75              | 2.15                   | 1.55                   | 75-225                          | 2.1-2.5, 2.7-3.1       | 65-315                          | 2.1-3.3                |
| 30                              | 2.1                                 | 49-51                        | 60                                       | 75                              | -0.950                | 40              | 2.15                   | 1.25                   | 65-155                          | 2.1-2.4                | 65-225                          | 2.1-2.8                |
| 30                              | 1.25                                | 0-100                        | $\infty$                                 | 80                              | -0.025                | 15              | 1.45                   | 1.15                   | 0-195                           | 1.25-2.3               | 0-375                           | 1.25-3.3               |
| 30                              | 1.25                                | 0-100                        | 200                                      | 80                              | -0.025                | 15              | 1.45                   | 1.15                   | 0-135                           | 1.25-1.9               | 0-255                           | 1.25-2.6               |
| 30                              | 1.25                                | 0-100                        | 130                                      | 80                              | -0.025                | 15              | 1.45                   | 1.15                   | 0-105                           | 1.3-1.8                | 0-195                           | 1.25-2.2               |
| 30                              | 1.25                                | 0-100                        | 60                                       | 70                              | -0.025                | 10              | 1.45                   | 1.15                   | 0-65                            | 1.3-1.6                | 0-105                           | 1.25-1.7               |
| 30                              | 1.25                                | 30-70                        | $\infty$                                 | 75                              | -0.025                | 20              | 1.45                   | 1.25                   | 0-175                           | 1.25-2.2               | 0-315                           | 1.25-3.1               |
| 30                              | 1.25                                | 30-70                        | 200                                      | 75                              | -0.025                | 20              | 1.45                   | 1.25                   | 0-135                           | 1.25-1.9               | 0-265                           | 1.25-2.8               |
| 30                              | 1.25                                | 30-70                        | 130                                      | 75                              | -0.025                | 20              | 1.45                   | 1.25                   | 0-115                           | 1.25-1.8               | 0-215                           | 1.25-2.5               |
| 30                              | 1.25                                | 30-70                        | 60                                       | 75                              | -0.025                | 20              | 1.45                   | 1.25                   | 0-75                            | 1.3-1.7                | 0-125                           | 1.25-1.9               |
| 30                              | 1.25                                | 49-51                        | $\infty$                                 | 90                              | -0.025                | 10              | 1.45                   | 1.25                   | 0-155                           | 1.25-2.2               | 0-305                           | 1.25-3.2               |
| 30                              | 1.25                                | 49-51                        | 200                                      | 90                              | -0.025                | 10              | 1.45                   | 1.25                   | 0-125                           | 1.25-1.9               | 0-255                           | 1.25-2.5, 2.9-2.1      |
| 30                              | 1.25                                | 49-51                        | 130                                      | 90                              | -0.025                | 10              | 1.45                   | 1.25                   | 0-105                           | 1.3-1.8                | 0-215                           | 1.25-2.4               |
| 30                              | 1.25                                | 49-51                        | 60                                       | 90                              | -0.025                | 10              | 1.45                   | 1.25                   | 0-85                            | 1.3-1.7                | 0-125                           | 1.25-1.8               |

lium star mass of  $1.25 M_\odot$  and Gaussian radial velocity distributions with velocity dispersions of more than  $130 \text{ km s}^{-1}$ , the PDFs favor kick directions opposite to the pre-SN orbital motion. In the case of the Gaussian radial velocity distribution with a velocity dispersion of  $60 \text{ km s}^{-1}$ , the PDF behaves qualitatively entirely different and shows a slight preference for kicks perpendicular to the pre-SN orbital velocity. A non-negligible low-probability tail furthermore extends well into the region of kick directions in the sense of the pre-SN orbital motion. When the minimum mass for pulsar B's pre-SN helium star progenitor is raised to  $2.1 M_\odot$ , the kicks are always directed opposite to the orbital motion (a lower

limit on  $\theta$  of  $\sim 113^\circ$  was already derived in Papers I and II). The PDF furthermore becomes fairly insensitive to the adopted radial velocity distribution.

Panel (f), finally, shows the distribution of possible pre-SN progenitor masses for different present-day radial velocity distributions, DNS ages of 0-100 Myr, and a minimum pre-SN helium star mass of  $1.25 M_\odot$ . The distributions all favor progenitor masses of  $1.4\text{--}1.5 M_\odot$ , with the preference for this mass range being strongest for present-day radial velocity distributions with small radial velocity dispersions. Distribution functions for a minimum pre-SN helium star mass of  $2.1 M_\odot$  look practically the same as the ones displayed panel (f) if they

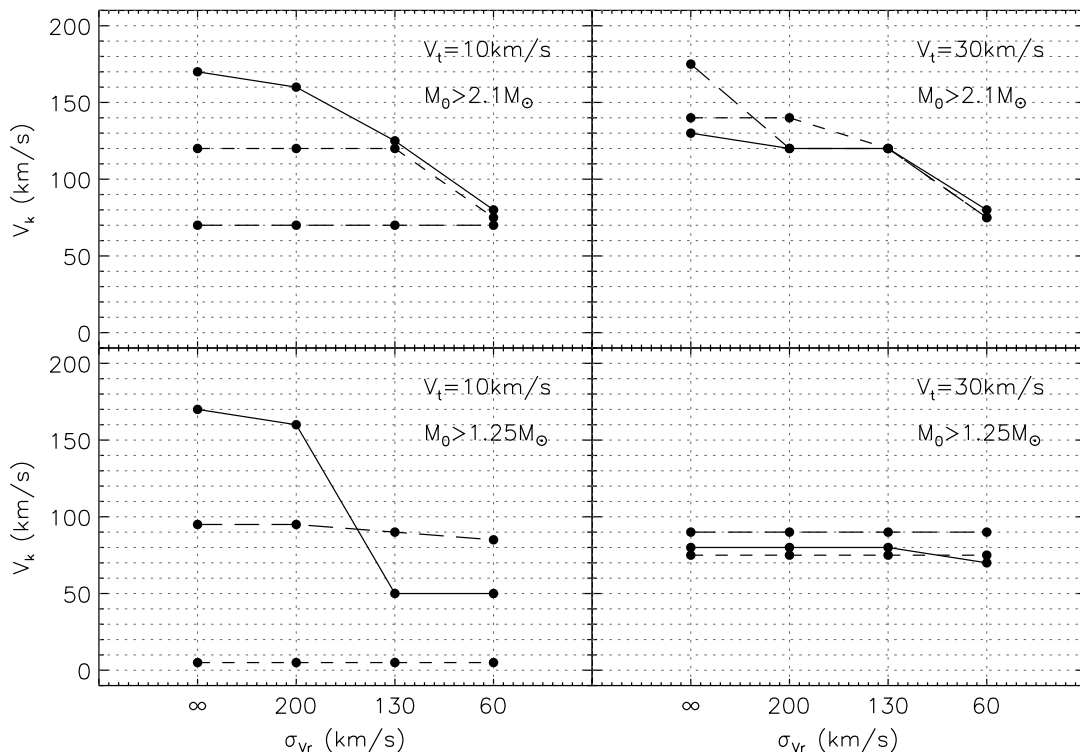


FIG. 4: Most likely SN kick velocity magnitude  $V_k$  for different sets of prior assumptions, for three age ranges: 0–100 Myr (solid lines), 30–70 Myr (short-dashed lines), 49–51 Myr (long-dashed lines). For brevity, the uniform radial velocity distribution is denoted by  $\sigma_{v_r} = \infty$ .

were cut off at  $2.1 M_{\odot}$ .

Adopting a present-day transverse velocity of  $30 \text{ km s}^{-1}$  instead of  $10 \text{ km s}^{-1}$  yields very similar conclusions. Overall the effects of varying model assumptions tend to be somewhat less pronounced though.

The 68% and 90% confidence limits on  $V_k$  and  $M_0$  obtained from the 1-D PDFs are listed in Table IV next to the most likely kick velocity and progenitor parameters [58]. In the majority of the cases, the confidence limits contain the most likely  $V_k$  and  $M_0$  obtained from the full 5-D PDF for  $V_k$ ,  $\cos\theta$ ,  $\phi$ ,  $M_0$ , and  $A_0$ . Whenever this is not the case, projection effects cause significant shifts between the values favored by the 1-D and 5-D PDFs. The confidence limits on  $V_k$  readily show that the possibility of small kick velocities is entirely due to the assumption that helium stars less massive than  $2.1 M_{\odot}$  can be viable NS progenitors. Under this assumption, the upper limits on  $V_k$  at the 68% confidence level vary from  $65 \text{ km s}^{-1}$  to  $275 \text{ km s}^{-1}$ . Thus, even though small kick velocities become possible, larger kick velocities in excess of  $100 \text{ km s}^{-1}$  are all but statistically disfavored. This is even more true when the upper limits at the 90% confidence level are considered. For a minimum pre-SN helium star mass of  $2.1 M_{\odot}$ , the confidence limits for  $V_k$  shift to significantly higher values which conform with the kick velocity magnitudes derived from observations of single radio pulsar [46–48]. These “conventional” kicks

are also consistent with the tilt between pulsar B’s rotation axis and the normal to the orbital plane inferred by Lyutikov & Thompson [49]. When the minimum pre-SN helium star mass is assumed to be  $1.25 M_{\odot}$ , the 68% and 90% confidence limits on  $M_0$  typically go all the way down to this limit, but often also extend upwards to masses larger than  $2.1 M_{\odot}$  (especially at the 90% confidence level). These numbers confirm our previous conclusion that the presently known observational constraints not necessarily disfavor progenitors more massive than  $2.1 M_{\odot}$  and kick velocities in excess of  $100 \text{ km s}^{-1}$ .

#### D. Birth sites

Just like the kick velocity and progenitor parameters, the most likely birth site of PSR J0737-3039B depends strongly on the adopted transverse systemic velocity component, age range, minimum helium star mass, and present-day radial velocity distribution. In § IV A, we have shown that the distribution of kinematic ages in the range from 0 to 100 Myr peaks strongly at ages of 1–2 Myr (see Fig. 2). This implies that the system can travel only a short distance (less than 2 kpc if the systemic velocity is less than  $1000 \text{ km s}^{-1}$ ) before reaching its current position. Adopting an age range of 0–100 Myr therefore yields PDFs for the birth sites that

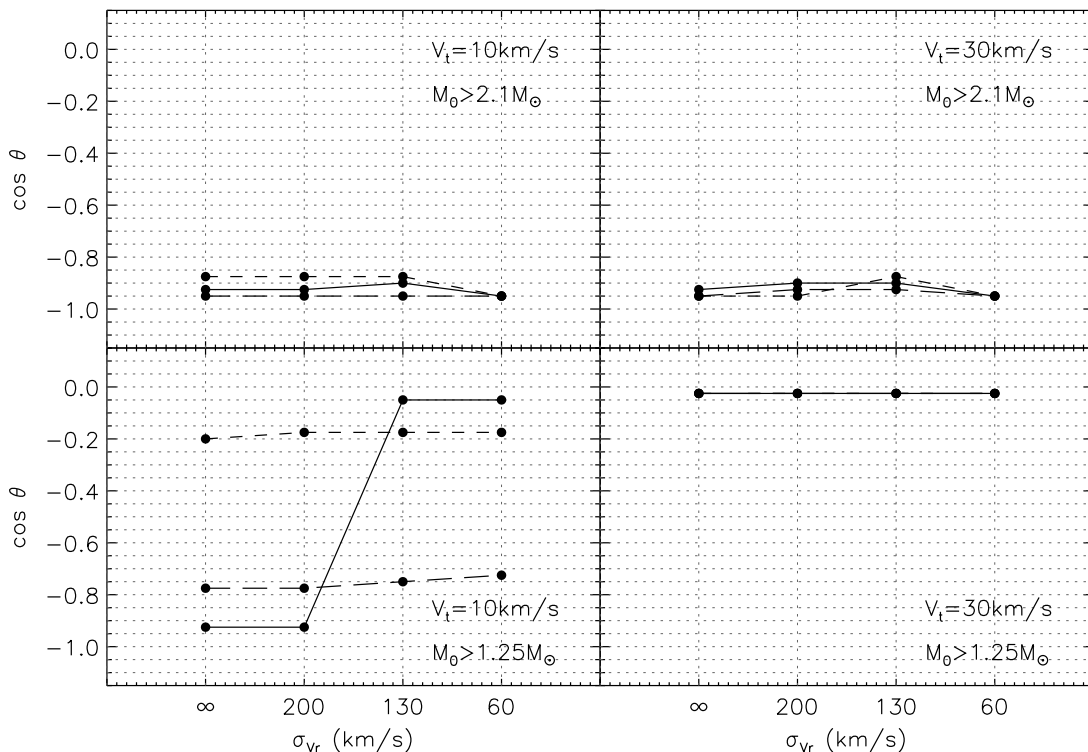


FIG. 5: Most likely SN kick direction  $\cos \theta$  for different sets of prior assumptions, for three age ranges: 0–100 Myr (solid lines), 30–70 Myr (short-dashed lines), 49–51 Myr (long-dashed lines). For brevity, the uniform radial velocity distribution is denoted by  $\sigma_{v_r} = \infty$ .

are strongly peaked near the system’s current position at  $X = -0.5$  kpc and  $Y = -8.3$  kpc, regardless of any of the other model assumptions. The situation changes drastically for the age ranges of 30–70 Myr and 49–51 Myr, which exclude very young ages and therefore impose a minimum distance traveled by the system since the time it was born.

For illustration, the distribution of the possible birth sites in the Galactic plane is shown in Fig. 8 in the case of a present-day transverse velocity component of  $30 \text{ km s}^{-1}$ , a minimum pre-SN helium star mass of  $1.25 M_{\odot}$ , an age range of 30–70 Myr, and a Gaussian radial velocity distribution with a velocity dispersion of  $130 \text{ km s}^{-1}$ . The most likely birth sites are all located within a radius of 2 kpc from  $(X, Y) = (-3.5, -7.5)$  kpc. None of the birth sites are furthermore close to the system’s present-day position indicated by the solid circle at  $(X, Y) = (-0.5, -8.3)$  kpc. If the minimum helium star mass required for NS formation is assumed to be  $2.1 M_{\odot}$  instead of  $1.25 M_{\odot}$ , the most likely birth sites shown in Fig. 8 become entirely inaccessible. Instead, the binary then most likely originates from a circle with a radius of 1 kpc centered on  $(X, Y) = (-2.5, -3.5)$  kpc, with a clear non-negligible lower probability tail extending more or less linearly towards  $(X, Y) = (3.5, 0.5)$  kpc.

## VII. COMPARISON WITH PREVIOUS WORK

### A. Willems et al. [15]

In Paper II, we derived constraints on the formation and progenitor of PSR J0737-3039B, using the then available observational constraints on the binary’s properties and motion in the Galaxy. The main differences with the observational and theoretical information adopted in this investigation are the lower transverse systemic velocity, the constraint on pulsar A’s spin-orbit misalignment angle, the possibility of a significantly lower minimum mass for pulsar B’s pre-SN helium star progenitor, and the use of DNS population synthesis calculations to obtain theoretical present-day radial-velocity distributions. Moreover, in Paper II we mainly focused on the ranges of possible progenitor parameters, and restricted the statistical analysis to the derivation of 1-D PDFs for pulsar B’s natal kick velocity and pulsar A’s spin-orbit misalignment. Among the observational and theoretical improvements, the availability of the constraint on pulsar A’s spin-orbit misalignment has the least effect on the derivation of the possible pulsar B progenitor and kick velocity properties. The main reason for this is that the excluded range of tilt angles from  $60^{\circ}$  to  $120^{\circ}$  was already statistically disfavored by the kick velocity and progenitor constraints derived in Paper II (see Fig. 12 in that paper).

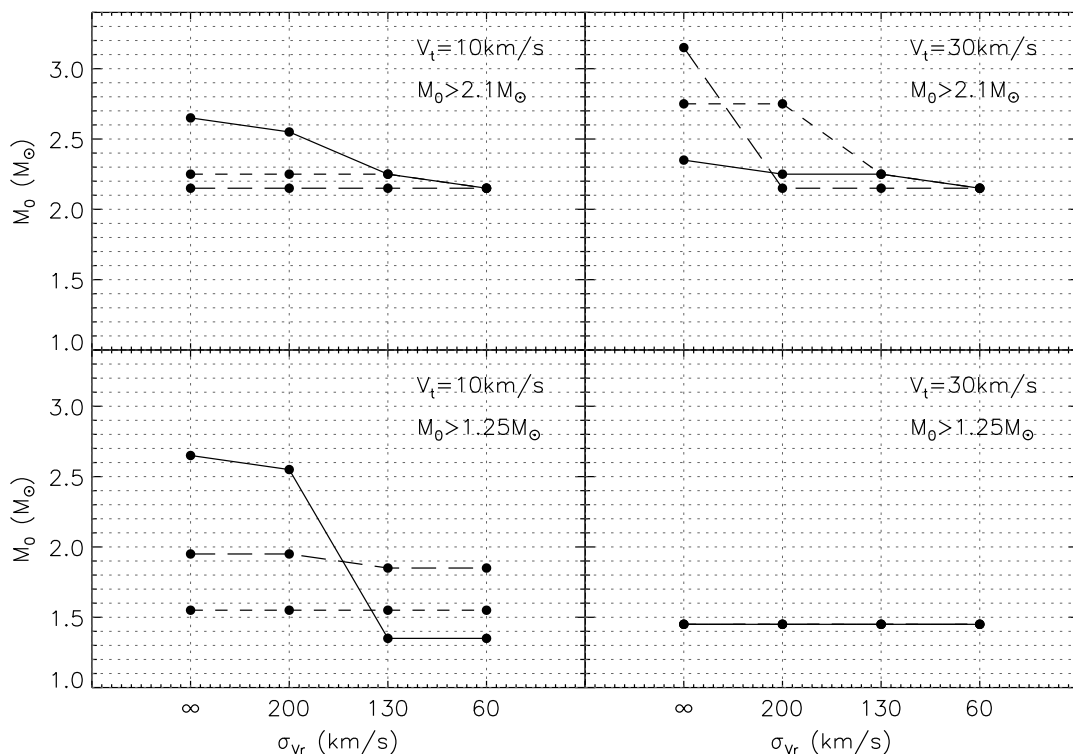


FIG. 6: Most likely pre-SN progenitor mass  $M_0$  for different sets of prior assumptions, for three age ranges: 0–100 Myr (solid lines), 30–70 Myr (short-dashed lines), 49–51 Myr (long-dashed lines). For brevity, the uniform radial velocity distribution is denoted by  $\sigma_{v_r} = \infty$ .

While the majority of the results presented in Paper II were obtained assuming a minimum pre-SN helium star mass of  $2.1 M_{\odot}$ , we also discussed some preliminary test calculations allowing pre-SN helium star masses below  $2.1 M_{\odot}$ . Because of the strong influence on the parameter space of the then available proper motion measurement of  $\sim 141 \text{ km s}^{-1}$ , we did not find any important changes in the kick velocity and progenitor constraints related to the decrease of the minimum admissible helium star mass. With the new proper motion upper limit of  $30 \text{ km s}^{-1}$ , the adopted minimum helium star mass has a much stronger effect on the available parameter space. In particular, when both the new proper motion constraint and the lower minimum helium star mass are imposed, there is no longer a lower limit on the magnitude of the kick velocity imparted to pulsar B at birth. Consequently a symmetric SN explosion becomes a viable formation mechanism for pulsar B. Moreover, allowing pre-SN helium star masses smaller than  $2.1 M_{\odot}$  also removes the lower limit of  $\sim 113^\circ$  on the angle between the kick velocity direction and the direction of the helium star’s pre-SN orbital velocity, so that the kicks no longer have to be directed opposite to the orbital motion.

## B. Piran & Shaviv [19, 20]

More recently, Piran & Shaviv [19, 20] (hereafter PS) used a Monte-Carlo method to argue that the probability of finding the system close to the Galactic plane is highest if pulsar B received only a marginal kick at birth of less than  $30 \text{ km s}^{-1}$ , and if its pre-SN progenitor had a very low mass of only about  $1.45 M_{\odot}$ . In their analysis, they considered the post-SN velocity of the binary randomly projected on the axis vertical to the Galactic plane (the  $Z$ -axis introduced in § IV A) and followed this one component of the Galactic motion forward in time for 50 Myr (their assumed age for PSR J0737-3039). However, restricting the Galactic motion to the  $Z$ -component can potentially bias the PDFs, since the horizontal velocity component remains entirely unconstrained (effectively, they accept all post-SN peculiar velocities as equally probable regardless of their horizontal component). In particular, if this horizontal component is large, it reduces the probability that the system would be found at its current  $X$  and  $Y$  position in a similar way as a large vertical component reduces the probability that the system is found at its current  $Z$  position. The analysis of PS furthermore implicitly assumes that the vertical motion is decoupled from the horizontal one. Although this is true locally, it is not true globally, since the vertical acceleration does not depend just on the ver-

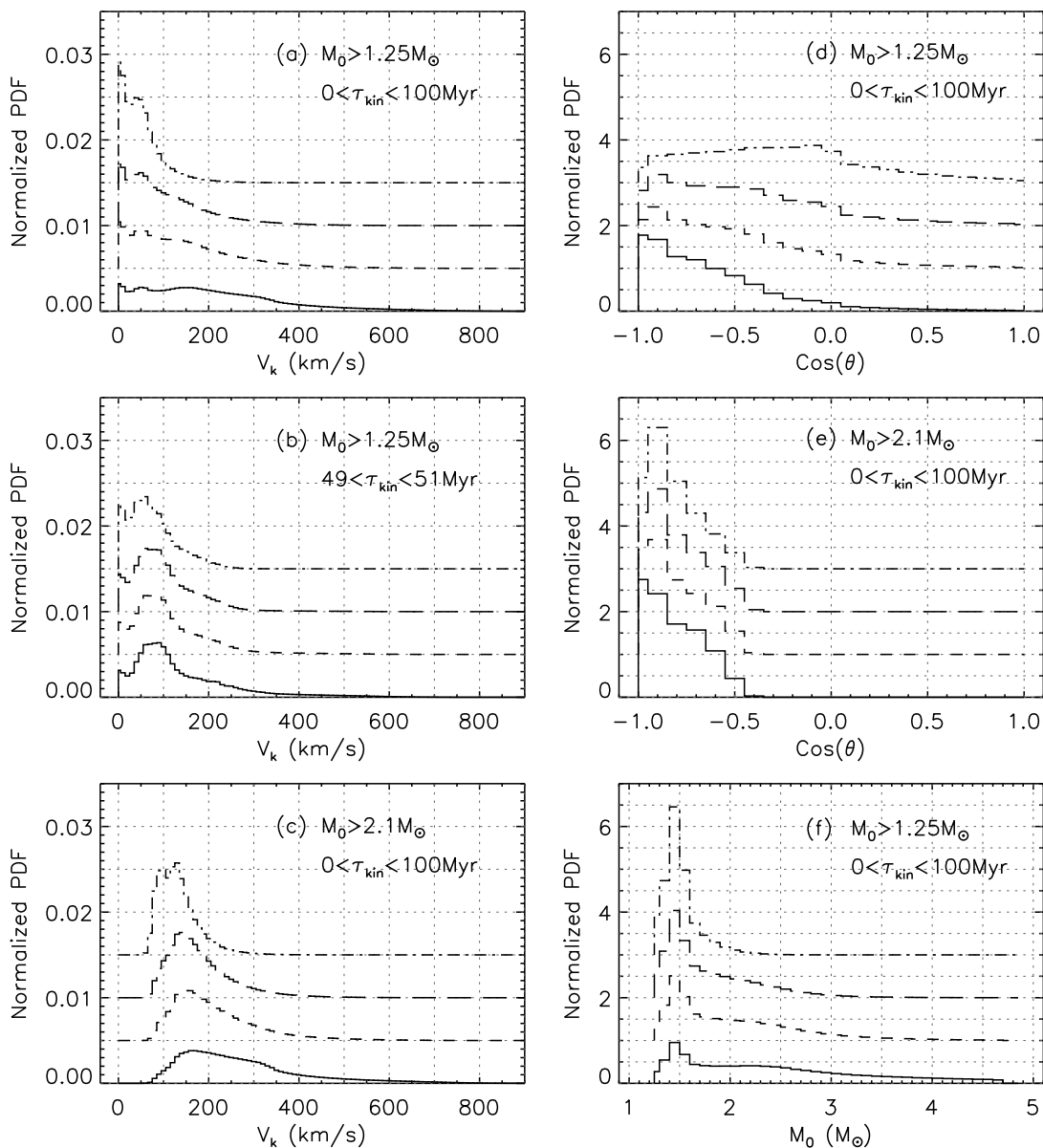


FIG. 7: One-dimensional PDFs illustrating some of the dependencies of the derived pulsar B kick velocity and progenitor properties on the adopted model assumptions. All plots are for a present-day transverse velocity of  $10 \text{ km s}^{-1}$ . Solid lines correspond to uniform radial velocity distributions and dashed lines to Gaussian distributions with velocity dispersions of  $60 \text{ km s}^{-1}$  (long-dashed lines),  $130 \text{ km s}^{-1}$  (short-dashed line), and  $200 \text{ km s}^{-1}$  (dash-dotted line). For clarity, the PDFs are offset from each other by an arbitrary amount. Panels (a)–(c) show the distributions of kick velocity magnitudes  $V_k$ , panels (d)–(e) the distributions of kick direction cosines  $\cos \theta$ , and panel (f) the distributions of pre-SN helium star masses  $M_0$ .

tical distance from the plane but also on the horizontal distance from the Galactic center. Therefore, if the binary has traveled through a wide range of Galactocentric radii, as indicated by the large range of possible birth sites displayed in Fig. 8, its vertical motion is different from the one modeled by PS.

We investigate this more thoroughly by following the steps outlined by PS. Firstly, we determine the post-SN orbital semi-major axis  $A$  and eccentricity  $e$  by integrating the equations governing the orbital evolution

due to gravitational wave emission backwards in time, for an assumed age of  $50 \text{ Myr}$ . We find  $A = 1.42 R_\odot$  and  $e = 0.105$ .

Secondly, we randomly generate a pulsar B kick velocity magnitude  $V_k$ , and kick direction angles  $\theta$  and  $\phi$ , assuming a uniform distribution for the magnitude and an isotropic distribution for the direction of the kick. Equations (4) and (5) and the associated constraints are then solved for  $M_0$  and  $A_0$ , using the values of  $A$  and  $e$  derived by reversing the orbital evolution for  $50 \text{ Myr}$  [59].



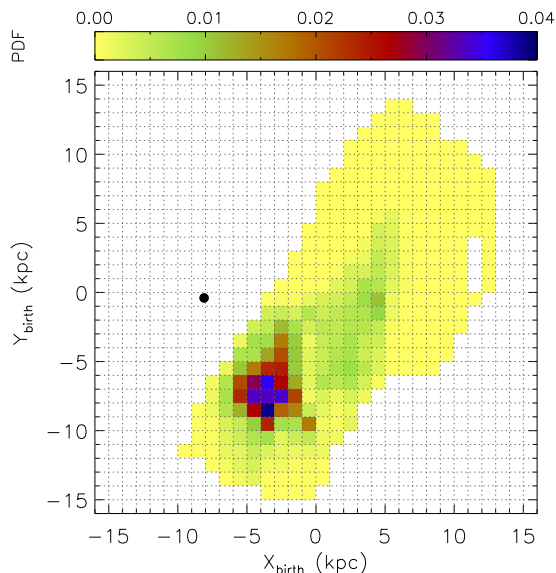


FIG. 8: Distribution of possible birth sites of PSR J0737-3039 in the Galactic plane for a transverse velocity component of  $30 \text{ km s}^{-1}$ , a minimum helium star mass of  $1.25 M_{\odot}$ , an age range of 30–70 Myr, and a Gaussian radial velocity distribution with a velocity dispersion of  $130 \text{ km s}^{-1}$ . The solid circle indicates the system’s present position.

If a solution for  $M_0$  and  $A_0$  exists, the magnitude of the post-SN peculiar velocity imparted to the binary’s center of mass is calculated by means of Eq. (6).

Thirdly, we approximate the motion of the system in the Galaxy by a local vertical oscillation with an amplitude drawn from a Gaussian distribution with a dispersion of 50 pc. At the time of the SN explosion, the system is assumed to be at a uniformly distributed random phase of the oscillation. The vertical motion of the system in the Galaxy is then followed forward in time for 50 Myr using the Galactic potential of Paczynski [45]. For this purpose, the randomly generated starting point has to be supplemented with the  $Z$ -component of the calculated post-SN peculiar velocity. Since the kick direction angles  $\theta$  and  $\phi$  are defined with respect to the pre-SN orbital plane, which has an unknown direction in space, the  $Z$ -component of the post-SN peculiar velocity is determined by assigning an isotropically distributed random direction to the calculated post-SN peculiar velocity. This new direction is generated with respect to the Galactic frame of reference  $OXYZ$  introduced in § IV A, and therefore straightforwardly leads to the determination of the  $Z$ -component of the post-SN peculiar velocity.

If the generated system satisfies all SN orbital dynamics constraints and if, after following the motion in the Galaxy for 50 Myr, the system ends up within 50 pc of the Galactic mid-plane, it is considered a possible progenitor of PSR J0737-3039 [60]. The procedure is then repeated until  $10^8$  such systems are found. The outcome of the simulation is a 2-D PDF of  $M_0$  and  $V_k$  shown in panel (a) of Fig. 9. The PDF is normalized so that

its integral over the entire admissible parameter space is equal to one. This is different from PS who normalize their PDF to the peak probability density [61]. The overall features of this PDF are to be compared to the upper right panel of Fig. 1 in Piran & Shaviv [19]; it is evident that the two PDFs are in rather good agreement. Differences in the details can be partly attributed to the PDF normalization adopted by PS (since it requires that the *exact* PDF peak is “captured” by the Monte Carlo process), which depends on the accuracy of the Monte-Carlo simulation and the size of the bins used to construct the PDF.

In order to assess the effect of approximating the space motion of PSR J0737-3039 as a vertical oscillation centered on the system’s current position, we repeated the above calculation for a system completely identical to the double pulsar, but located at a different position in the Galactic plane. In particular, we positioned the system closer to the Galactic center at  $X = -2.5 \text{ kpc}$  and  $Y = -3.5 \text{ kpc}$  (this corresponds to the most likely birth site found in § VI for a present-day transverse velocity of  $30 \text{ km s}^{-1}$ , an age of 30–70 Myr, a Gaussian radial velocity distribution with a velocity dispersion of  $130 \text{ km s}^{-1}$ , and a minimum pre-SN helium star mass of  $2.1 M_{\odot}$ ). Somewhat surprisingly, we found the effect on the PDFs to be rather minimal. As a second test, we therefore considered a second system identical to the double pulsar, but located at a height of  $790 \pm 50 \text{ pc}$  above the Galactic plane (corresponding to the distance of PSR B1534+12 to the Galactic plane). Again, we found minimal changes in the PDF. We conclude that the position of the system in the Galaxy therefore seems to be relatively unimportant in the derivation of the  $(V_k, M_0)$ -PDF.

This conclusion is further strengthened by the results in panel (b) of Fig. 9: it shows the 2-D PDF obtained *without any* constraint on  $|Z|$ . It is evident that the PDF does not depend in any significant way on the position of PSR J0737-3039 close to the Galactic plane, in contrast to what is claimed by PS (the main difference between panels (a) and (b) is that the “peak” contour is somewhat more spread out). Indeed when tracking the progenitor systems as they are affected by the different constraints in the simulations, we find that the  $|Z| < 50 \text{ pc}$  constraint eliminates only 13% of the systems that satisfy all other imposed constraints. It turns out that the orbital dynamics of asymmetric SN explosions and associated constraints are much more important than the position of the system in the Galaxy in determining the  $(V_k, M_0)$ -PDF.

For comparison, we also constructed 2-D kick velocity and progenitor mass distributions by marginalizing the 5-D PDFs derived in § VI, for model assumptions similar to those adopted by Piran & Shaviv [20]. Specifically, we considered a present-day transverse velocity of  $30 \text{ km s}^{-1}$ , a minimum helium star mass of  $1.25 M_{\odot}$ , kinematic ages of 49–51 Myr, and a Gaussian radial velocity distribution with a dispersion of  $130 \text{ km s}^{-1}$ . We also removed the limits on pulsar A’s spin-orbit misalignment from the list

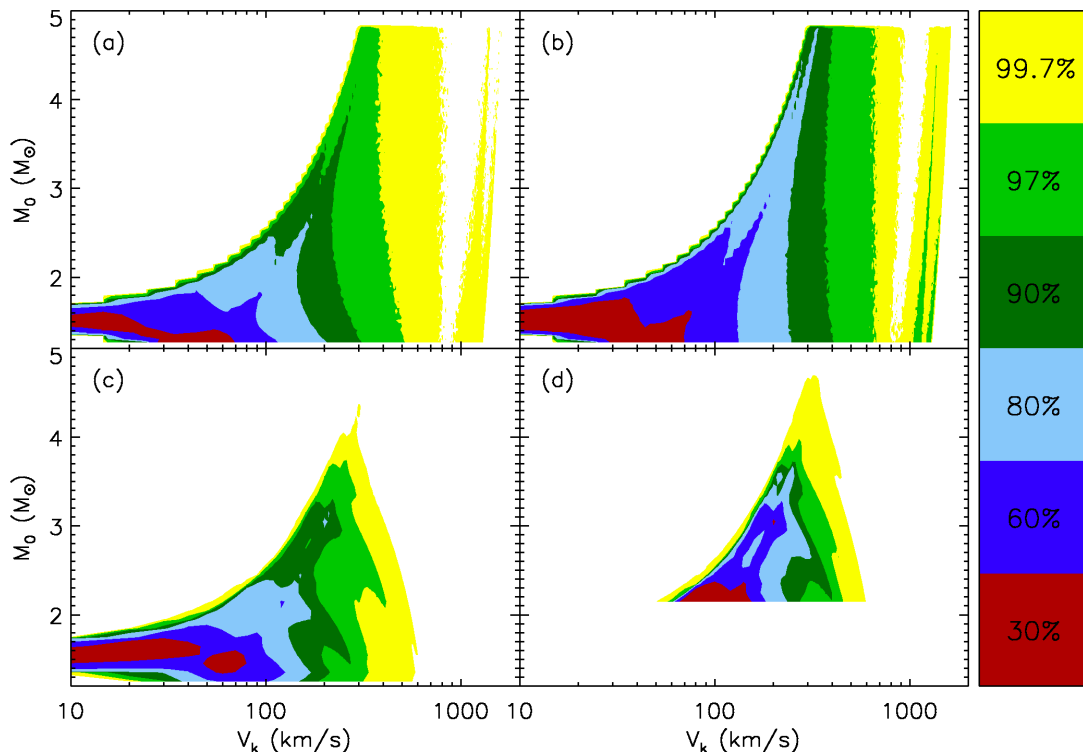


FIG. 9: Contour plots for the  $(V_k, M_0)$ -PDF. Panels (a) and (b) correspond to the PDFs obtained using the method outlined by PS. The PDF shown in Panel (a) only includes systems with  $|Z| \lesssim 50$  pc, while the PDF shown in panel (b) does not incorporate any constraints on the position of the system in the Galaxy. Panels (c) and (d) correspond to the PDFs obtained using the method outlined in this paper. The PDF shown in panel (c) corresponds to a present-day transverse velocity of  $30 \text{ km s}^{-1}$ , a minimum pre-SN helium star mass of  $1.25 M_\odot$ , kinematic ages of 49–51 Myr, and a Gaussian radial velocity distribution with a dispersion of  $130 \text{ km s}^{-1}$ . The PDF shown in panel (d) adopts the same assumptions, except that the minimum pre-SN helium star mass is assumed to be  $2.1 M_\odot$ .

of imposed constraints as it was not incorporated in the analysis of PS. The resulting PDF is shown in panel (c) of Fig. 9. We note that, although the analysis by PS does not incorporate the radial velocity, it is an indispensable part of our method which cannot be omitted from the analysis. A comparison between our results and those derived by PS with exactly the same assumptions is therefore not possible. Despite this, the differences between the PDFs displayed in panels (a) and (c) are quite minimal. The same holds true if the Gaussian radial velocity distribution with a dispersion of  $130 \text{ km s}^{-1}$  is replaced by any of the other radial-velocity distributions considered. In view of the non-negligible differences between the two approaches, this agreement is all but trivial and thus strengthens our confidence in the validity of the derived results. The effect of the minimum helium star mass on the PDF is illustrated in panel (d), where the minimum pre-SN helium star mass was assumed to be  $2.1 M_\odot$ . The main difference with the PDF shown in panel (c) is the minimum kick velocity of  $\sim 60 \text{ km s}^{-1}$ . The most likely kick velocity is of the order of  $60\text{--}100 \text{ km s}^{-1}$  and the most likely progenitor mass is  $2.1\text{--}2.4 M_\odot$ .

Thus, we conclude that (i) if one allows *a priori* for low-mass progenitors of pulsar B, and (ii) if the marginalized

2-D PDF is considered and not the underlying 5-D PDF, then the preference for low progenitor masses and low kicks is rather generic and it is not related to the system’s position close to the plane or the small upper limit on the proper motion in any crucial way (c.f. PS). This applies to both the analysis presented in this paper and the analysis by PS. Examining the role of the prior assumptions and considering the full 5-D PDF of  $V_k$ ,  $\cos\theta$ ,  $\phi$ ,  $M_0$ , and  $A_0$  are therefore essential in establishing an unbiased view of the possible formation mechanism and progenitor of PSR J0737-3939B.

Finally, we note that, contrary to what is claimed by PS, small tilt angles between pulsar A’s spin angular momentum and the post-SN orbital angular momentum do not necessarily imply that a small SN kick was imparted to pulsar B at birth. This can, e.g., be seen from Figs. 11 and 12 in Paper II. In addition, Eq. (7) shows that the tilt depends on the direction as well as on the magnitude of the natal kick velocity, and that in the particular case where the kicks are confined to the pre-SN orbital plane, the tilt angle is equal to zero regardless of the magnitude of the kick velocity.

## VIII. SUMMARY AND CONCLUDING REMARKS

In this study, we have considered the kinematic and evolutionary history of the double pulsar PSR J0737-3039, taking into account the most up-to-date observational constraints. Unlike our earlier work on this topic, we focus here on the derivation of the full multi-dimensional probability distribution functions for the magnitude and direction of the kick velocity imparted to pulsar B at birth, the mass of pulsar B’s pre-SN helium star progenitor, and the pre-SN orbital separation. The consideration of the multi-dimensional PDF has the distinct advantage that it is free of projection effects and that it accounts for all possible correlations between the derived parameters; these correlations and projection effects turn out to be very important when addressing the question of what are the most likely properties of the double pulsar’s progenitor. We also examine the dependence of the PDFs on the prior assumptions for the magnitude of the transverse systemic velocity component, the minimum pre-SN helium star mass required to form a NS, the age of the system, and the present-day radial velocity. Since the latter cannot be determined from observation, we construct and explore theoretical radial-velocity distributions by means of population synthesis calculations for coalescing DNSs.

One of the main results of our analysis is that marginalizing the full five-dimensional progenitor PDF to 1-D or 2-D distributions for the pulsar B kick velocity and progenitor mass has a major effect on the determination of their most likely values. When the full multi-dimensional PDF is examined, it is clear that although some sets of prior assumptions indeed favor low kick velocities and low progenitor masses, as claimed by Piran & Shaviv [19], the majority of the models favor kick velocities of 50–180 km s<sup>-1</sup> and progenitor masses of 1.45–2.75  $M_{\odot}$ .

In particular, if the transverse systemic velocity is assumed to be 30 km/s and helium stars less massive than 2.1  $M_{\odot}$  are assumed to be viable NS progenitors, the most likely pulsar B progenitor mass is 1.45  $M_{\odot}$  regardless of any of the other prior assumptions. If, on the other hand, the transverse systemic velocity is assumed to be 10 km/s while keeping the assumption that helium stars less massive than 2.1  $M_{\odot}$  are viable NS progenitors, the most likely progenitor mass can vary from 1.35  $M_{\odot}$  to 2.65  $M_{\odot}$ , depending on the assumed systemic age and radial velocity distribution. Hence, whether progenitor masses greater than 2.1  $M_{\odot}$  are statistically likely or unlikely depends strongly on the adopted prior assumptions (cf. [19, 20]). Most likely progenitors with  $M_0 < 2.1 M_{\odot}$  can furthermore also be associated with kick velocities of up to 100 km s<sup>-1</sup> (see, e.g., the case of  $V_t = 30$  km s<sup>-1</sup> and  $M_0 > 1.25 M_{\odot}$  in Figs. 4 and 6), while kick velocities of less than 60 km s<sup>-1</sup> are only possible for progenitor masses below 2.1  $M_{\odot}$ .

We also find that the proximity of PSR J0737-3039 to the Galactic plane and the small proper motion do not

pose stringent constraints on the kick velocity and progenitor mass of pulsar B. Instead, the constraints are predominantly determined by the orbital dynamics of asymmetric SN explosions. This is in contrast to the work of Piran & Shaviv [19, 20] who emphasize that the proximity of the double pulsar to the Galactic plane implies that pulsar B most likely received only a small kick at birth and that its progenitor most likely had mass of  $\sim 1.45 M_{\odot}$ .

Hence, based on the currently available observational constraints, a wide range of progenitor and kick velocity properties are favored for PSR J0737-3039B. In particular, the constraints are compatible with a conventional hydrodynamical or neutrino-driven SN explosion from a helium star more massive than 2.1  $M_{\odot}$  [10, 41], as well as an electron-capture SN from a helium star less massive than 2.5  $M_{\odot}$  [50, 51]. Podsiadlowski et al. [3] have speculated that the electron-capture SN mechanism may be typical for close binaries and that it may be accompanied by much smaller kicks than hydrodynamical or neutrino-driven SN explosions. Consequently, if pulsar B is formed through an electron capture SN and if electron capture SNe are accompanied by small kicks, the mass of pulsar B’s pre-SN helium star progenitor must be smaller than 2.1  $M_{\odot}$  (otherwise the kick is always larger than  $\sim 60$  km s<sup>-1</sup>). Since it is unlikely that future observations will lead to new constraints on the smallest possible pulsar B progenitor mass, further insight to the formation mechanism of pulsar B should be sought in core-collapse simulations of low-mass ( $\lesssim 2.1 M_{\odot}$ ) helium stars and population synthesis studies of PSR J0737-3039-type binaries and their progenitors.

### Acknowledgments

We are grateful to Laura Blecha for sharing the code used to calculate the Galactic motion of PSR J0737-3039 backwards in time, and to Richard O’Shaughnessy for useful discussions on multi-dimensional statistics. This work is partially supported by a NSF Gravitational Physics grant PHY-0353111, a David and Lucile Packard Foundation Fellowship in Science and Engineering grant, and NASA ATP grant NAG5-13236 to VK; and a Northwestern University Summer Research Grant to JK. KB acknowledges the support of KBN grant 1P03D02228.

### APPENDIX A: COMMENTS BY PIRAN & SHAVIV ON THIS WORK

Piran & Shaviv [21] recently posted a Comment on the astro-ph preprint server “refuting” the work presented in this paper. Their argumentation, however, rests on severe misstatements of our analysis and neglects some of the major conclusions drawn in the previous sections. While we have already addressed their criticism at ap-

appropriate places throughout this paper, we here wish to summarize our counterarguments to eliminate any further misunderstandings:

(1) Our results are not "in spite of the observations" as claimed by Piran & Shaviv [21]. They are based on all currently available observational constraints, most of which are in fact initial conditions in our calculation.

(2) While we do conclude that most of our models yield kick velocities of 50–180 km s<sup>-1</sup>, we do not claim that the models favoring lower kick velocities are less likely. We conclude even less that the most likely pulsar B progenitor mass is large. It can, e.g., be seen from Table IV that if the transverse systemic velocity is assumed to be 30 km/s and the minimum pulsar B progenitor mass is assumed to be 1.25  $M_{\odot}$ , the most likely progenitor mass is 1.45  $M_{\odot}$  regardless of any of the other prior assumptions. If, on the other hand, the transverse systemic velocity is assumed to be 10 km/s while the minimum progenitor mass is kept at 1.25  $M_{\odot}$ , the most likely progenitor mass can vary from 1.35  $M_{\odot}$  to 2.65  $M_{\odot}$ , depending on the assumed age range and radial velocity distribution. Our main conclusion is thus that the prior assumptions play an important role in determining the most likely kick velocity and progenitor properties.

(3) We do not assume that the system is moving with a very large velocity almost exactly towards. Instead, we adopt theoretical radial-velocity distributions based on realistic binary evolution models for coalescing DNSs that reside close to the Galactic plane and have small transverse systemic velocity components, consistent with the current observational constraints on the kinematics of the double pulsar. Because of the latter constraints, the distributions implicitly incorporate the geometrical probability argument put forward in Eq. (2) of [21]. We furthermore also consider four different distribution functions (one flat distribution and three Gaussians of varying width) in order to assess the robustness of our results

(see, e.g., Table IV).

(4) The differences between our conclusions and those of Piran & Shaviv [19] rest on the consideration of the full 5-D PDF instead of a marginalized 2-D one, not on the modeling of the motion of the system in Galaxy. The reason for this is that the orbital parameters and the dynamics of asymmetric SN explosions turn out to be much more constraining than the system's position and motion in the Galaxy (contrary to what is claimed by Piran & Shaviv [19]). Piran & Shaviv [21] also completely miss that when we adopt similar assumptions as they do, and marginalize our 5-D PDFs for  $V_k$ ,  $\cos\theta$ ,  $\phi$ ,  $M_0$ , and  $A_0$  to 2-D PDFs for  $M_0$  and  $V_k$ , we find results that are in excellent agreement with theirs, irrespective of the treatment of the unknown radial velocity.

(5) The population synthesis calculations used to construct the theoretical radial-velocity distributions incorporate the possibility that mass transfer takes place right before the formation of pulsar B. The models therefore allow the pre-SN masses of helium stars in DNS progenitors to be as low as the 1.45  $M_{\odot}$  pulsar B progenitor mass favored by Piran & Shaviv [19]. The derived radial-velocity distributions are thus by no means biased towards high progenitor masses as claimed by Piran & Shaviv [21].

(6) Based on the preceding arguments, the conclusion of Piran & Shaviv [21] that "we assume the result we obtain" clearly rests on severe misinterpretations of the calculations underlying our analysis.

We want to conclude this discussion by stressing that the goal of our paper is not to refute the progenitor and kick constraints derived by Piran & Shaviv [19]. We do however want to make it clear that there are many additional factors that were not considered by these authors, and that these may affect the determination of the most likely progenitor and kick velocity properties.

- 
- [1] Burgay, M., et al. 2003, *Nature (London)*, 426, 531  
 [2] Lyne, A. G., et al. 2004, *Science*, 303, 1153  
 [3] Podsiadlowski, P., Dewi, J. D. M., Lesaffre, P., Miller, J. C., Newton, W. G., & Stone, J. R. 2005, *Monthly Notices of the Royal Astronomical Society*, 361, 1243  
 [4] Kramer, M., et al. 2005, *ArXiv Astrophysics e-prints*, arXiv:astro-ph/0503386  
 [5] Kalogera, V., et al. 2004, *Astrophys. J. Letters*, 601, L179  
 [6] Kalogera, V., et al. 2004, *Astrophys. J. Letters*, 614, L137  
 [7] Bhattacharya, D., & van den Heuvel, E. P. J. 1991, *Physics Reports*, 203, 1  
 [8] Brown, G. E. 1995, *Astrophys. J.*, 440, 270  
 [9] Belczynski, K., Kalogera, V., & Bulik, T. 2002, *Astrophys. J.*, 572, 407  
 [10] Tauris, T. M., & van den Heuvel, E. 2006, *ArXiv Astrophysics e-prints*, arXiv:astro-ph/0303456  
 [11] Belczyński, K., & Kalogera, V. 2001, *Astrophys. J. Letters*, 550, L183  
 [12] Belczynski, K., Bulik, T., & Kalogera, V. 2002, *Astrophys. J. Letters*, 571, L147  
 [13] Dewi, J. D. M., & van den Heuvel, E. P. J. 2004, *Monthly Notices of the Royal Astronomical Society*, 349, 169  
 [14] Willems, B., & Kalogera, V. 2004, *Astrophys. J. Letters*, 603, L101 (Paper I)  
 [15] Willems, B., Kalogera, V., & Henninger, M. 2004, *Astrophys. J.*, 616, 414 (Paper II)  
 [16] Ransom, S. M., Kaspi, V. M., Ramachandran, R., Demorest, P., Backer, D. C., Pfahl, E. D., Ghigo, F. D., & Kaplan, D. L. 2004, *Astrophys. J. Letters*, 609, L71  
 [17] Coles, W. A., McLaughlin, M. A., Rickett, B. J., Lyne, A. G., & Bhat, N. D. R. 2005, *Astrophys. J.*, 623, 392  
 [18] Manchester, R. N., et al. 2005, *Astrophys. J. Letters*, 621, L49  
 [19] Piran, T., & Shaviv, N. J. 2005, *Physical Review Letters*,

- 94, 051102
- [20] Piran, T., & Shaviv, N. J. 2005, ArXiv Astrophysics e-prints, arXiv:astro-ph/0510584
- [21] Piran, T., & Shaviv, N. J. 2006, ArXiv Astrophysics e-prints, arXiv:astro-ph/0603649
- [22] Kalogera, V. 2000, *Astrophys. J.*, 541, 319
- [23] Kramer, M., Lyne, A. G., Hobbs, G., Löhmer, O., Carr, P., Jordan, C., & Wolszczan, A. 2003, *Astrophys. J. Letters*, 593, L31
- [24] Lyutikov, M. 2004, *Monthly Notices of the Royal Astronomical Society*, 353, 1095
- [25] Lorimer, D. R., et al. 2004, ArXiv Astrophysics e-prints, arXiv:astro-ph/0404274
- [26] Pfahl, E., Rappaport, S., Podsiadlowski, P., & Spruit, H. 2002, *Astrophys. J.*, 574, 364
- [27] Chen, B., et al. 2001, *Astrophys. J.*, 553, 184
- [28] Carlberg, R. G., & Innanen, K. A. 1987, *Astronomical Journal*, 94, 666
- [29] Kuijken, K., & Gilmore, G. 1989, *Monthly Notices of the Royal Astronomical Society*, 239, 571
- [30] Cordes, J. M., Romani, R. W., & Lundgren, S. C. 1993, *Nature (London)*, 362, 133
- [31] Chatterjee, S., et al. 2005, *Astrophys. J. Letters*, 630, L61
- [32] Belczynski, K., Kalogera, V., Rasio, F. A., Taam, R. E., Zezas, A., Bulik, T., Maccarone, T. J., & Ivanova, N. 2005, ArXiv Astrophysics e-prints, arXiv:astro-ph/0511811
- [33] Kalogera, V., Narayan, R., Spiegel, D. N., & Taylor, J. H. 2001, *Astrophys. J.*, 556, 340
- [34] Junker, W., & Schäfer, G. 1992, *Monthly Notices of the Royal Astronomical Society*, 254, 146
- [35] Hills, J. G. 1983, *Astrophys. J.*, 267, 322
- [36] Brandt, N., & Podsiadlowski, P. 1995, *Monthly Notices of the Royal Astronomical Society*, 274, 461
- [37] Kalogera, V. 1996, *Astrophys. J.*, 471, 352
- [38] Fryer, C., & Kalogera, V. 1997, *Astrophys. J.*, 489, 244
- [39] Kalogera, V., & Lorimer, D. R. 2000, *Astrophys. J.*, 530, 890
- [40] Willems, B., Henninger, M., Levin, T., Ivanova, N., Kalogera, V., McGhee, K., Timmes, F. X., & Fryer, C. L. 2005, *Astrophys. J.*, 625, 324
- [41] Habets, G. M. H. J. 1986, *Astronomy & Astrophysics*, 167, 61
- [42] Ivanova, N., Belczynski, K., Kalogera, V., Rasio, F. A., & Taam, R. E. 2003, *Astrophys. J.*, 592, 475
- [43] Dewi, J. D. M., Pols, O. R., Savonije, G. J., & van den Heuvel, E. P. J. 2002, *Monthly Notices of the Royal Astronomical Society*, 331, 1027
- [44] Dewi, J. D. M., & Pols, O. R. 2003, *Monthly Notices of the Royal Astronomical Society*, 344, 629
- [45] Paczynski, B. 1990, *Astrophys. J.*, 348, 485
- [46] Hobbs, G., Lorimer, D. R., Lyne, A. G., & Kramer, M. 2005, *Monthly Notices of the Royal Astronomical Society*, 360, 974
- [47] Zou, W. Z., Hobbs, G., Wang, N., Manchester, R. N., Wu, X. J., & Wang, H. X. 2005, *Monthly Notices of the Royal Astronomical Society*, 362, 1189
- [48] Faucher-Giguere, C. -A., & Kaspi, V. M. 2005, ArXiv Astrophysics e-prints, arXiv:astro-ph/0512585
- [49] Lyutikov, M., & Thompson, C. 2005, *Astrophys. J.*, 634, 1223
- [50] Nomoto, K. 1984, *Astrophys. J.*, 277, 791
- [51] Nomoto, K. 1987, *Astrophys. J.*, 322, 206
- [52] From Fig. 6 in Belczynski et al. [9] it follows that less than 2% of the systems have a peculiar velocity larger than  $100 \text{ km s}^{-1}$  after the first SN explosion.
- [53] This is assuming the Sun is located at a height of 30 pc above the Galactic plane [see, e.g., 27]
- [54] In Paper II, the motion of the system in the Galaxy backwards in time was accidentally calculated for the wrong set of current Galactic coordinates. Due to the system's proximity to the Sun ( $d \sim 0.6 \text{ kpc}$ ) this error mainly affected the appearance of Figs. 3–5, but not the derived ranges of kinematic ages and post-SN peculiar velocities. Correspondingly, the derived constraints on the mass of pulsar B's pre-SN helium star progenitor, the pre-SN orbital separation, the magnitude and direction of pulsar B's natal kick velocity, and the probability distributions for the kick magnitude and spin-orbit misalignment angle are also largely unaffected.
- [55] This uniform distribution is what we also assumed in Paper II. Piran & Shaviv [20] incorrectly state that the results presented in Paper I are dictated by the implicit assumption that the system is moving with a large radial velocity towards us. The kick velocity and progenitor parameters derived in Paper I are, however, based solely on stellar and binary evolution considerations. Constraints on the proper motion did not become available until the writing of Paper II in which we presented the possible kick velocity and progenitor parameters *as a function* of the unknown radial velocity. In that paper, we considered the full range of radial velocities, from small to large, as having a flat distribution function.
- [56] In kinematic calculations of DNS binaries the part of the motion preceding the second supernova explosion is most often ignored as negligible. However, we have examined our radial velocity distributions with and without this early motion and we can confirm that its effect is indeed negligible. This is not so much due to the somewhat smaller center-of-mass velocities after the first explosion (compared to those after the second explosion because of the wide orbits involved); instead it is mostly due to the very short time between the two events (from about one tenth to a few Myr).
- [57] An updated population synthesis study on coalescing DNSs shows that some systems can actually survive the dynamically unstable mass-transfer phase and form a DNS (Belczynski et al., in preparation). In view of our conservative upper limit of  $4.7 M_{\odot}$  on the mass of pulsar B's pre-SN helium star progenitor and the small values of our PDFs for masses near this upper limit, we do not expect this possibility to significantly affect the results presented in this paper.
- [58] Confidence limits for  $\cos\theta$ ,  $\phi$ , and  $A_0$  were also calculated but these did not contribute any significant new information.
- [59] Note that PS consider a range of eccentricities  $0.088 < e < 0.14$  obtained by reversing the past orbital evolution for a range of ages between 0 Myr and 210 Myr (the characteristic age of *pulsar A*). Although, this is inconsistent with the age of 50 Myr adopted for the Galactic motion calculations, we do not expect the use of the range of eccentricities to have a strong impact on the derivation of the  $V_k$ ,  $\cos\theta$ ,  $\phi$ ,  $M_0$ , and  $A_0$  constraints. It is furthermore unclear if PS solve Eqs. (4) and (5) by randomly generating eccentricities from a uniform distribution between 0.088 and 0.14, or by some other unspecified procedure.

For these reasons, we modify this step in PS's analysis and consistently use the post-SN orbital parameters associated with a fixed age of 50 Myr.

[60] Contrary to PS, we do not impose any constraint on the present-day transverse systemic velocity, since there is no unambiguous way to impose the constraint without making additional assumptions about the system's present-day 3-D space velocity. In particular, limiting the motion of the system in the Galaxy to a local vertical oscillation restricts the knowledge of the velocity in the simulations

to the component perpendicular to the Galactic plane. Since this component does not lay in the plane perpendicular to the line-of-sight to the double pulsar, imposing the proper motion constraint requires additional assumptions on the radial velocity and the direction of the proper motion.

[61] Because of the chosen normalization, the contour levels in PS measure the decrease of the PDF with respect to its maximum value. They therefore do not correspond to confidence levels.